SIAM J. DISCRETE MATH.
Vol. 32, No. 1, pp. 750–782
© 2018 Society for Industrial and Applied Mathematics

ON THE OPTIMALITY OF THE FCC LATTICE FOR SOFT SPHERE PACKING*

HERBERT EDELSBRUNNER† AND MABEL IGLESIAS-HAM†

Abstract. Motivated by biological questions, we study configurations of equal spheres that neither pack nor cover. Placing their centers on a lattice, we define the soft density of the configuration by penalizing multiple overlaps. Considering the 1-parameter family of diagonally distorted 3-dimensional integer lattices, we show that the soft density is maximized at the FCC lattice.

Key words. packing and covering, soft density, lattice configurations, Voronoi domains, Brillouin zones

AMS subject classifications. 05B40, 52C17, 11H31

DOI. 10.1137/16M1097201

1. Introduction.

High-resolution microscopic observations of the DNA organization inside the nucleus of a human cell support the *Spherical Mega-base-pairs Chromatin Domain model* [7, 19]. It proposes that inside the chromosome territories of eukaryotic cells, DNA is compartmentalized into sequences of highly interacting segments of about the same length [9]. Each segment consists of roughly a million base pairs and is rolled up to resemble a round ball. The balls are tightly arranged within the available space, tighter than a packing since the balls deform when pressed against each other, and less tight than a covering so that protein machines can find access to the DNA needed for gene expression.

Motivated by the mentioned biological findings, the authors of [18] consider configurations of spheres in which the overlap is limited by a parameter, and the quality of the configuration is measured by its *density*, which is the expected number of balls that contain a randomly selected point. Writing φ_i for the probability that a randomly selected point lies in at least i balls, the density is $\delta = \sum_{i \geq 1} \varphi_i$. Computational experiments reported in the same paper show that for small values of the parameter, the highest density is attained for the FCC lattice, and that for large values, the highest density is attained for the BCC lattice. These experiments are limited to a 1-parameter family of lattices—the same considered in this paper—and it is remarkable that there is a sharp transition, with none of the other lattices challenging the dominance of FCC and BCC. A similar setting was considered in [2] but for different reasons. To study the packing of balls, the authors give upper bounds on the volume of the union in which every ball is thickened by a parameter. Equivalently, the (thickened) balls are packed softly, allowing for a limited overlap controlled by the parameter. The bounds are proved for packings in $\mathbb{R}^n$ and are not limited to lattices. Soft packing is also the natural setting for modeling physical processes at the nanoscale. For example, Radin [21] considers finitely many interacting particles governed by a potential function defined for pairs that penalizes distances below a

*Received by the editors October 4, 2016; accepted for publication (in revised form) January 8, 2018; published electronically March 29, 2018.
http://www.siam.org/journals/sidma/32-1/M109720.html
Funding: This work was partially supported by the DFG Collaborative Research Center TRR 109, "Discretization in Geometry and Dynamics," through grant I02979-N35 of the Austrian Science Fund (FWF).
†IST Austria (Institute of Science and Technology Austria), 3400 Klosterneuburg, Austria (edels@ist.ac.at, miglesias@ist.ac.at).

threshold while giving preference to particles in close contact but above the distance threshold. In two dimensions, the optimal configuration was found to be a subset of the hexagonal lattice. As an alternative to parametrizing the overlap, the authors of [11] measure a configuration by the probability of a randomly selected point to belong to exactly one ball. In $\mathbb{R}^2$, this measure attains its maximum for the hexagonal grid [1, 11], and even nonlattice configurations cannot increase the measure [4].

The interested reader can find a wealth of further information and references on packing and covering in [6, 17]. To avoid ambiguity, we mention that in the mathematical literature, a *packing* refers to a configuration of balls (hard spheres) with disjoint interiors, while a *covering* is one in which the balls cover the entire space without gaps. The traditional measure of quality is the density as defined above.

In this paper, we restrict our attention to equal balls centered at points of a lattice. Departing from [2, 18] and also [11], we introduce the *soft density*, $\delta_1 = \varphi_1 - \sum_{i\geq 2} \varphi_i$, which penalizes for gaps in the coverage but also for overlaps among the balls. Following [12], we focus on the 1-parameter *diagonal family* of lattices obtained by compressing or stretching the integer lattice along the diagonal direction. We use the unimodality of the measure to prove the following optimality result in $\mathbb{R}^3$.

THEOREM 1 (main result). *Among the lattices in the diagonal family in* $\mathbb{R}^3$*, the FCC lattice with balls of radius* $1.090\ldots$ *times the packing radius maximizes the soft density at* $\delta_1 = 0.844\ldots$.

The proof of Theorem 1 is a detailed study of all lattices in the diagonal family, giving analytic expressions for the maximum soft density over distortion intervals that cover the entire family. Crucial ingredients to the proof are the use of Brillouin zones, a new result about their long-range behavior in lattices, and the unimodality of the soft density.

Outline. Section 2 discusses lattice configurations, generalized Voronoi domains, and Brillouin zones. Section 3 introduces the soft density measures and shows that their restrictions to fixed lattices are unimodal. Section 4 presents the case analysis that proves Theorem 1. Section 5 concludes the paper.

2. Lattice configurations. In $\mathbb{R}^n$, we need n linearly independent vectors to define a *lattice*, which consists of all integer combinations:

$$\Lambda(a_1, a_2, \ldots, a_n) = \left\{ p = \sum_{i=1}^{n} k_i a_i \mid k_i \in \mathbb{Z} \right\}. \tag{1}$$

Note that 0 is a point in $\Lambda = \Lambda(a_1, a_2, \ldots, a_n)$ and that the neighborhood of every lattice point looks like the neighborhood of every other lattice point. We will therefore focus on 0 and its neighborhood.

2.1. Voronoi domains and Brillouin zones. A standard tool in the study of lattices is the *Voronoi diagram*, which assigns to each point $p \in \Lambda$ the set of points $x \in \mathbb{R}^n$ for which p is the closest lattice point or, if there is a tie, p is among the closest lattice points. This set is a convex polyhedron and is commonly referred to as the *Voronoi domain* of p. We are interested in short- and long-range interactions between the points, which motivates us to generalize this concept.

Perpendicular bisectors. Following Fejes Toth [15, 16], we define the ith Voronoi domain of 0 as the set of points $x \in \mathbb{R}^n$ for which 0 is among the i nearest lattice points, denoting this domain by $V_i(0)$. We write $V(0) = V_1(0)$ for the ordinary Voronoi domain.

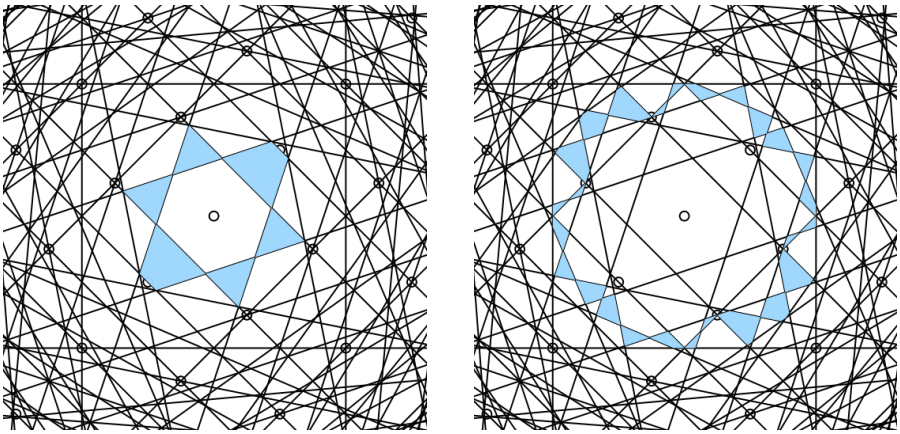

FIG. 1. *Drawing all bisectors defined by* 0 *and other points in the lattice, we get the* i*th Brillouin zone of* 0 *as the closure of the points separated from* 0 *by* $i-1$ *of the bisectors. We highlight the second Brillouin zone on the* left *and the sixth Brillouin zone on the* right. *Related to this concept is the* i*th Voronoi domain of* 0*, which is the union of the first* i *Brillouin zones or, equivalently, the closure of the points separated from* 0 *by* $i-1$ *or fewer lines.*

There are at least two rather different ways to construct these domains; see Figure 1 for an illustration of the first. Recall that the *perpendicular bisector* of $p \neq q$ is the hyperplane of points at equal distance from both: $\|x-p\| = \|x-q\|$. Drawing all perpendicular bisectors defined by 0 and $p \in \Lambda \setminus \{0\}$, we get an arrangement of countably many hyperplanes in $\mathbb{R}^n$. The hyperplanes decompose $\mathbb{R}^n$ into *chambers*, which are maximal closed sets so that no two points lie on opposite sides of any of the hyperplanes. For example, $V(0)$ is the unique chamber that contains 0. Every other chamber is separated from 0 by at least one hyperplane, and $V_i(0)$ is the union of all chambers separated from 0 by at most $i-1$ hyperplanes.

The generalized Voronoi domains are not necessarily convex, but they satisfy a related weaker condition. A set $A \subseteq \mathbb{R}^n$ is *star-convex* if there exists a point $a \in A$ such that for every $x \in A$ the entire line segment connecting a to x is contained in A. The *kernel* of A is the set of such points a, which is a subset of A.

LEMMA 2 (star-convexity). *Let* Λ *be a lattice in* $\mathbb{R}^n$*. For each* $i \geq 1$*,* $V_i(0)$ *is bounded and star-convex, and* 0 *lies in the interior of its kernel.*

Proof. Because Λ is a lattice, there is a real number $R = R(i)$ such that every ball of radius R contains i or more lattice points in its interior. It follows that no point $x \in V_i(0)$ can be at distance R or further from 0. In other words, $V_i(0)$ is bounded. It is star-convex because $x \in V_i(0)$ implies that all points on the line segment connecting x to 0 belong to $V_i(0)$. Indeed, if x is separated by at most $i-1$ bisectors from 0, then so is any point on this line segment. This also proves that 0 belongs to the kernel of $V_i(0)$. But this is still true if we substitute any point of the first Voronoi domain for 0, so the entire $V(0)$ belongs to the kernel, which implies that 0 belongs to the interior of the kernel, as claimed. ∎

It is often convenient to consider the difference between two contiguous domains rather than individual domains. Following the French physicist Léin Brillouin (see [5]), we therefore define $Z_i(0)$ as the closure of $V_i(0) \setminus V_{i-1}(0)$, calling it the *ith Brillouin zone* centered at 0. Setting $V_0(0) = \emptyset$, the first zone is $Z_1(0) = V(0)$.

Zone invariants. Fixing i, we note that the ith Brillouin zones of different lattice points have disjoint interiors, and the collection of all ith zones covers $\mathbb{R}^n$. Incidentally, this is the *degree-i Voronoi diagram* as defined in [14]. Since any two ith zones are translates of each other, and because there are equally many ith zones as there are jth zones—namely one for each lattice point—it must be that all Brillouin zones have the same volume. This result was mentioned already by Bieberbach [3]. We formalize this insight and generalize it to measures beyond the n-dimensional volume. Recall that a function $\mu\colon \mathbb{R}^n \to \mathbb{R}$ is *integrable* if

$$\mu[B] = \int_{x\in B} \mu(x)\,\mathrm{d}x \tag{2}$$

is well defined for every Borel set $B \subseteq \mathbb{R}^n$. It is Λ-*periodic* if $\mu(x) = \mu(x+p)$ for every $x \in \mathbb{R}^n$ and every $p \in \Lambda$. For example, if μ is identical 1, then it is obviously periodic and $\mu[B]$ is the n-dimensional volume of B. We prove that every Brillouin zone has the same measure, no matter what center or index.

THEOREM 3 (zone invariants). *Let Λ be a lattice in $\mathbb{R}^n$ and $\mu\colon \mathbb{R}^n \to \mathbb{R}$ be a Λ-periodic integrable function. Then $\mu[Z_i(p)] = \mu[Z_j(q)]$ for all $i, j \geq 1$ and all $p, q \in \Lambda$.*

Proof. In a lattice, every point looks like every other point: $\Lambda = \Lambda + p$ for every $p \in \Lambda$. For a point $p \in \Lambda$, we have $Z_i(p) = Z_i(0) + p$, and because μ is Λ-periodic, $\mu[Z_i(p)] = \mu[Z_i(0)]$ for every $i \geq 1$. By transitivity,

$$\mu[Z_i(p)] = \mu[Z_i(q)] \tag{3}$$

for all $p, q \in \Lambda$ and all $i \geq 1$. To extend this relation to Brillouin zones with different indices, we consider the closed ball with radius $R > 0$ centered at the origin, denoted by $B(0, R)$. Counting the lattice points in the ball with $m(R) = \operatorname{card}(B(0,R) \cap \Lambda)$, we write $\Omega_i(R)$ for the union of the ith zones centered at these $m(R)$ points. Letting w_i be the maximum distance of a point $x \in Z_i(0)$ from 0, we note that the symmetric difference between $B(0, R)$ and $\Omega_i(R)$ is contained inside the annulus of points at distance at most w_i on either side of the sphere that bounds $B(0, R)$. With increasing R, the volume of this annulus grows asymptotically slower than the volume of the ball. Hence,

$$\mu[Z_i(0)] = \frac{\mu[\Omega_i(R)]}{m(R)} = \lim_{R\to\infty} \frac{\mu[B(0,R)]}{m(R)}. \tag{4}$$

The right-hand side converges to a finite value that is independent of i. It follows that the measure of any ith zone is the same as the measure of any jth zone. The claimed relation thus follows from (3) and (4). ∎

Example 1. Fixing a nonnegative integer j, set $\mu(x) = 1$ if x is covered by j or more balls, and set $\mu(x) = 0$ otherwise. Clearly, μ is a periodic integrable function, so Theorem 3 implies that the volume of points covered by at least j balls is the same within every Brillouin zone. For $j = 0$, this formalizes our informal argument that all zones have the same n-dimensional volume.

Example 2. Let μ have Dirac deltas at the lattice points. More concretely, let $\epsilon > 0$ be sufficiently small, and set

$$\mu(x) = \max_{p\in\Lambda} \left\{0, \tfrac{(n+1)(\epsilon - \|x-p\|)}{\nu_n \epsilon^{n+1}}\right\}, \tag{5}$$

in which ν_n is the n-dimensional volume of the unit ball. Clearly, μ is a periodic integrable function and $\mu[V(0)] = 1$. Theorem 3 implies that the measure of every zone is 1. Interpreting this measure as counting lattice points, we get exactly one lattice point per zone, provided we take appropriate fractions if the points are shared.

2.2. Iterative construction. The second way of constructing the generalized Voronoi domains proceeds in rounds of invasions and relocations of conquered real-estate. We remark that Sibson used the same "area-stealing" idea to construct interpolations based on Voronoi diagrams [22].

Invasion and relocation. We construct the second Brillouin zone centered at 0 by letting the Voronoi neighbors invade $V(0)$ and divide up the real-estate. Each obtained region belongs to an ordered pair, $(0, p)$, in which 0 and p are the first and second lattice points from any point in the region. Translating the region to the Voronoi domain of $-p$, we get $Z_2(0)$ as the union of these regions; see Figure 2.

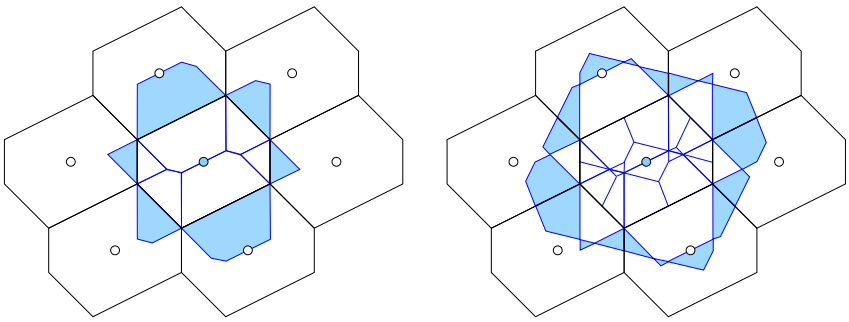

FIG. 2. Left: *We decompose the first Voronoi domain of* 0 *according to the second nearest lattice point and assemble the second Brillouin zone by moving each piece to the reflection of the corresponding point.* Right: *We refine the decomposition according to the third nearest lattice point and assemble the third Brillouin zone by moving each piece to the reflection of the corresponding point.*

We can iterate. Specifically, we further decompose each region by letting the surrounding regions invade and divide up the real-estate, as before. Each region in this decomposition belongs to an ordered triplet, $(0, p, q)$, in which $0, p, q$ are the first, second, and third lattice points from any point in the region. Translating the region to the Voronoi domain of $-q$, we get $Z_3(0)$ as the union of these regions, as before; see again Figure 2.

Piecewise translations. We formalize the iterative construction by proving that there is a piecewise translation from $V(0)$ to $Z_i(0)$ for every i. To describe this map, let x be a point in $V(0)$. Ordering the lattice points in increasing distance from x, we get $\|x - p_1\| \leq \|x - p_2\| \leq \cdots \leq \|x - p_i\| \leq \cdots$. Most of these inequalities are strict, and ties are broken arbitrarily. For $i \geq 1$, we define $f_i \colon V(0) \to Z_i(0)$ by mapping x to $f_i(x) = x - p_i$. We will show that f_i is *almost* a bijection. To express this, we let $V_i^\circ \subseteq V(0)$ be the set of points x in $V(0)$ for which the first and ith lattice points are unique: $\|x - p_1\| < \|x - p_2\|$ and $\|x - p_{i-1}\| < \|x - p_i\| < \|x - p_{i+1}\|$. Similarly, we let $Z_i^\circ \subseteq Z_i(0)$ be the set of points in the ith Brillouin zone for which the first and ith lattice points are unique. Note that V_i° is contained in the interior of $V(0)$ and contains almost all points of the Voronoi domain. Similarly, Z_i° is contained in the interior of $Z_i(0)$ and contains almost all points of the ith Brillouin zone.

LEMMA 4 (bijection). *For each $i \geq 1$, the restriction of the function f_i to $V_i^\circ \subseteq V(0)$ and $Z_i^\circ \subseteq Z_i(0)$ is a bijection.*

Proof. First we show that the restriction of f_i is well defined. Recall that 0 and p_i are the unique first and ith lattice points from x. Since $f_i(x) = x - p_i$, this implies that $0 - p_i = -p_i$ and $p_i - p_i = 0$ are the unique first and ith lattice points from $f_i(x)$. It follows that $f_i(x)$ belongs to the interior of $V(-p_i)$ as well as to the interior of $Z_i(0)$, and thus to Z_i°.

To prove that the restriction is injective, let $p_i, p_i' \in \Lambda$ be the ith lattice points from $x, x' \in V_i^\circ$. If $p_i = p_i'$, then $f_i(x) - f_i(x') = x - x'$, so that $x \neq x'$ implies $f_i(x) \neq f_i(x')$. Otherwise, if $p_i \neq p_i'$, we have $f_i(x) \neq f_i(x')$ because the two points lie in the interiors of two different first Voronoi domains.

To prove that f_i is surjective, we start with a point y in Z_i° and let $p \in \Lambda$ such that $y \in V(-p)$. Define $x = y + p$. Since $-p$ and 0 are the unique first and ith lattice points from y, this implies that $-p + p = 0$ and $0 + p = p$ are the unique first and ith lattice points from x. Hence, x belongs to V_i° and $f_i(x) = y$. ∎

It is not difficult to see that the functions f_i can be used to give a second proof of Theorem 3. Indeed, the restriction of f_i to V_i° and Z_i° is a bijection that consists of finitely many translations. Each translation maps a connected piece of V_i° to a connected piece of Z_i°. By the periodicity of μ, the measure of these two pieces is the same. Since the pieces are pairwise disjoint and cover almost all of $V(0)$ and of $Z_i(0)$, this implies that $\mu[V(0)] = \mu[Z_i(0)]$. We get the relation in Theorem 3 by transitivity.

2.3. Configurations of balls. We call a set of closed balls in $\mathbb{R}^n$ a *configuration of balls* or, equivalently, a *configuration of spheres* if we want to emphasize how the boundaries of the balls decompose space. We are interested in the case in which all balls have the same radius and the centers are placed periodically in $\mathbb{R}^n$. Letting $B(p, r) = B(0, r) + p$ be the closed ball with radius $r > 0$ centered at $p \in \mathbb{R}^n$, we write

$$\mathcal{B}(\Lambda, r) = \{B(p, r) \mid p \in \Lambda\} \tag{6}$$

for the configuration of balls defined by the lattice and the radius. In this subsection, we fix Λ as well as r and write $\mathcal{B} = \mathcal{B}(\Lambda, r)$.

Multiple covering. For each $i \geq 0$, let $\mathbb{B}_i \subseteq \mathbb{R}^n$ be the set of points that are covered by at least i of the balls in $\mathcal{B}$. For finite r, there is a minimum index, m, such that $\mathbb{B}_i = \emptyset$ iff $i \geq m$. Clearly, $\emptyset = \mathbb{B}_m \subseteq \cdots \subseteq \mathbb{B}_1 \subseteq \mathbb{B}_0 = \mathbb{R}^n$. To assess the relative size of these sets, we let φ_i be the probability that a randomly selected point in $\mathbb{R}^n$ is contained in at least i of the balls. More formally,

$$\varphi_i(\Lambda, r) = \lim_{R \to \infty} \frac{\mathrm{vol}[\mathbb{B}_i \cap B(0, R)]}{\mathrm{vol}[B(0, R)]} = \frac{\mathrm{vol}[\mathbb{B}_i \cap V(0)]}{\mathrm{vol}[V(0)]}, \tag{7}$$

in which we get the right-hand side because $\mathbb{B}_i$ intersects every Voronoi domain in the same way. The inclusions among the $\mathbb{B}_i$ imply that $0 = \varphi_m \leq \cdots \leq \varphi_1 \leq \varphi_0 = 1$. Observe also that $\varphi_i - \varphi_{i+1}$ is the probability that a randomly selected point lies in exactly i balls of $\mathcal{B}$.

Probability in terms of volume. We generalize (7) by considering the intersections of $B(0, r)$ with the generalized Voronoi domains: $D_i(r) = B(0, r) \cap V_i(0)$, for $i \geq 0$, noting that $D_0(r) = V_0(0) = \emptyset$. Continuing the convention of dropping the fixed

radius from the notation, we write $D_i = D_i(r)$.

LEMMA 5 (probability). *For each $i \geq 1$, the probability that a randomly selected point in $\mathbb{R}^n$ belongs to at least i balls in $\mathcal{B}$ is*

$$\varphi_i = \frac{\text{vol}[D_i] - \text{vol}[D_{i-1}]}{\text{vol}[V(0)]}. \tag{8}$$

Proof. Let x be a point in $V(0)$. We prove the claimed relation by showing that the point $y = f_i(x)$ belongs to $D_i \setminus D_{i-1}$ iff x is covered by at least i balls; see Figure 3. This implies (8). We now prove the two directions of the claimed equivalence.

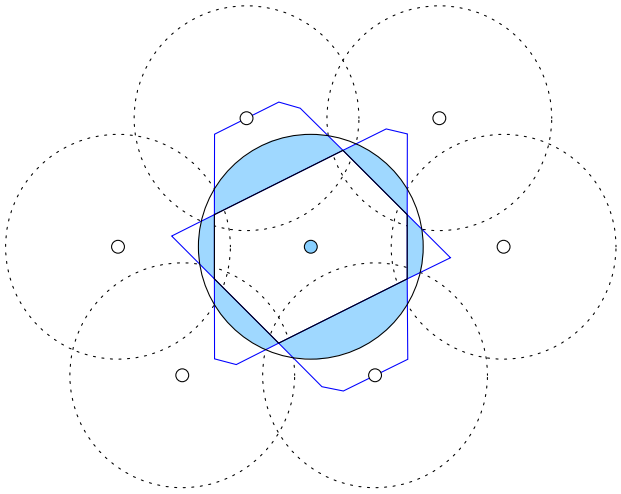

FIG. 3. *The probability that a randomly selected point is covered by at least two disks is the normalized area of the intersection between the disk centered at* 0 *and the second Brillouin zone of* 0. *Indeed, we can move the pieces of this intersection back into the first Voronoi domain so that they decompose the portion covered by at least two disks, the one centered at* 0 *and the other centered at a neighboring lattice point.*

"$\Longrightarrow$". By construction of the function, $y = f_i(x)$ belongs to $Z_i(0)$. If it furthermore belongs to $B(0, r)$ and thus to $D_i \setminus D_{i-1}$, then 0 is the ith lattice point from y and its ball covers y. Hence, y is covered by at least i balls, which implies that x is covered by at least i balls.

"$\Longleftarrow$". If x is covered by at least i balls, then so is $y = f_i(x)$. We have $y \in Z_i(0)$ by definition, and $y \in B(0, r)$ because 0 is the ith lattice point from y. Hence, $y \in D_i \setminus D_{i-1}$. ∎

3. Measures of density. Given a lattice configuration of balls, the classic notion of *density* is the expected number of balls that contain a randomly selected point:

$$\delta(\Lambda, r) = \sum_{i \geq 1} \varphi_i = \frac{\text{vol}[B(0, r)]}{\text{vol}[V(0)]}, \tag{9}$$

in which the ratio on the right-hand side is clear and also follows from Lemma 5. We introduce variants of this classic notion that penalize for overlapping balls and prove that for a fixed lattice they are unimodal functions of the radius.

3.1. Soft densities. In this subsection, we introduce a family of soft densities and relate them to volumes of balls and generalized Voronoi domains.

Two definitions. Let $\Lambda \subseteq \mathbb{R}^n$ be a lattice and $r > 0$ be a radius. For each $j \geq 1$, we define the *jth soft density* of $\mathcal{B} = \mathcal{B}(\Lambda, r)$ as

$$\delta_j(\Lambda, r) = \sum_{i=1}^{j} \varphi_i - \sum_{i=j+1}^{\infty} \varphi_i. \tag{10}$$

We have $\delta_1 \leq \delta_2 \leq \cdots \leq \delta$, and $\delta_j = \delta$ iff the configuration does not have any $j+1$ overlapping balls.

From the point of view of the applications motivating the work described in this paper, the most interesting soft density is the first: $\delta_1(\Lambda, r) = \varphi_1 - \varphi_2 - \varphi_3 - \ldots$. It favors configurations of balls with only minor overlap. Nonetheless, there are lattices for which the configuration that maximizes the first soft density has triplets of overlapping balls. To avoid the complications caused by triple intersections, we introduce the first simplified soft density:

$$\delta_{1\mathrm{s}}(\Lambda, r) = \sum_{i=1}^{\infty} (3 - 2i)\varphi_i, \tag{11}$$

noting that $\delta_{1\mathrm{s}} \leq \delta_1$ agree on the first two terms and differ only in the weight given to overlaps of three or more balls. We will see shortly that $\delta_{1\mathrm{s}}$ is easier to compute than δ_1.

Density in terms of volume. Recall that (9) writes the classic notion of density as the normalized volume of a ball. We generalize this relation to soft densities, unsimplified and simplified.

LEMMA 6 (soft density). *Let $j \geq 1$. The jth soft density and the first simplified soft density of the configuration of balls defined by a lattice Λ and a radius r are*

$$\delta_j = \frac{2\mathrm{vol}[D_j] - \mathrm{vol}[B(0,r)]}{\mathrm{vol}[V(0)]}, \tag{12}$$

$$\delta_{1\mathrm{s}} = \frac{\mathrm{vol}[B(0,r)]}{\mathrm{vol}[V(0)]} - \sum_{0 \neq p \in \Lambda} \frac{\mathrm{vol}[B(0,r) \cap B(p,r)]}{\mathrm{vol}[V(0)]}. \tag{13}$$

Proof. We first prove the relation for the unsimplified soft densities. Writing the two normalized volumes on the right-hand side of (12) in terms of probabilities, we get

$$\frac{\mathrm{vol}[D_j]}{\mathrm{vol}[V(0)]} = \sum_{i=1}^{j} \varphi_i, \tag{14}$$

$$\frac{\mathrm{vol}[B(0,r)]}{\mathrm{vol}[V(0)]} = \sum_{i=1}^{\infty} \varphi_i. \tag{15}$$

Taking the first sum twice and subtracting the second sum, we match the definition of the jth soft measure in (10).

Second, we prove the relation for the simplified soft density. Equation (15) writes the first normalized volume in (13) in terms of probabilities. To do the same for the second normalized volume, we note that the common intersection of $B(0,r)$ and $k-1$ other balls is accounted for $k-1$ times. Recall that $B(0,r) \cap \mathbb{B}_k$ is the subset of the

ball covered by at least $k-1$ other balls. The second normalized volume in (13) can therefore be rewritten as

$$\mathrm{V}_{\mathrm{Lunes}} = \sum_{k=2}^{\infty} \frac{\mathrm{vol}[B(0,r) \cap \mathbb{B}_k]}{\mathrm{vol}[V(0)]} = \sum_{k=2}^{\infty} \sum_{i=1}^{\infty} \frac{\mathrm{vol}[Z_i(0) \cap B(0,r) \cap \mathbb{B}_k]}{\mathrm{vol}[V(0)]}, \tag{16}$$

in which we get the second line by decomposing the ball into its intersections with the Brillouin zones. To write the double-sum in terms of probabilities, we note that the indicator function of $\mathbb{B}_k$ is Λ-periodic. Hence, Theorem 3 implies that

$$\frac{\mathrm{vol}[Z_i(0) \cap \mathbb{B}_k]}{\mathrm{vol}[V(0)]} = \varphi_k \tag{17}$$

for all choices of $i \geq 1$ and $k \geq 0$. Recall now that for every point $x \in Z_i(0)$, the origin is the ith lattice point from x. For $1 \leq i \leq k$, 0 is among the first k lattice points. Hence, if x is contained in k or more balls, then it is also contained in $B(0,r)$. For $k \leq i$, $x \in Z_i(0)$ is contained in $B(0,r)$ iff it is contained in i or more balls. Hence,

$$\frac{\mathrm{vol}[Z_i(0) \cap B(0,r) \cap \mathbb{B}_k]}{\mathrm{vol}[V(0)]} = \begin{cases} \varphi_k & \text{for } 1 \leq i \leq k, \\ \varphi_i & \text{for } k \leq i, \end{cases} \tag{18}$$

in which we get the first line from (17) and the second line from (8). Starting with (13), we use (15) to rewrite the first sum and combine (16) with (18) to rewrite the second sum to get

$$\delta_{1\mathrm{s}} = \sum_{i=1}^{\infty} \varphi_i - \sum_{k=2}^{\infty} \left(k\varphi_k + \sum_{i=k+1}^{\infty} \varphi_i \right) = \sum_{i=1}^{\infty} (3-2i)\varphi_i. \tag{19}$$

Simple rearrangements lead to the right-hand side, which matches the definition of the first simplified density in (11). ∎

3.2. Derivatives. In this subsection, we fix the lattice but vary the radius. It is therefore convenient to write $\mathcal{B}(r) = \mathcal{B}(\Lambda, r)$, $\delta_j(r) = \delta_j(\Lambda, r)$, etc. We are interested in the radius at which a soft density attains its maximum.

Derivative of probability. Since all density measures in this paper are linear combinations of probabilities, we focus on the functions $\varphi_i \colon \mathbb{R}_+ \to \mathbb{R}$. Remembering that $\varphi_i(r)$ is the normalized volume of $B(0,r) \cap Z_i(0)$, we introduce radii $r_i < R_i$ such that this intersection is empty iff $r < r_i$ and equal to $Z_i(0)$ iff $R_i \leq r$. Specifically, r_i is the supremum of the radii for which every ball contains fewer than i lattice points, and R_i is the supremum of the radii for which there exists a center such that the ball contains fewer than i lattice points. For example, r_2 is the packing radius of Λ, and R_1 is the covering radius of Λ. Within the interval $[r_i, R_i]$, φ_i increases monotonically from 0 to 1. When we increase the radius, the volume of $B(0,r) \cap Z_i(0)$ grows where the sphere $\partial B(0,r)$ lies inside $Z_i(0)$. To streamline the notation, we write $S_i(r) = \partial B(0,r) \cap V_i(0)$, and we write $\mathrm{area}[S_i(r)]$ for its $(n-1)$-dimensional volume. Recalling that the ith Brillouin zone is $Z_i(0) = V_i(0) \setminus V_{i-1}(0)$, we therefore get

$$\frac{\partial \varphi_i}{\partial r}(r) = \frac{\mathrm{area}[S_i(r)] - \mathrm{area}[S_{i-1}(r)]}{\mathrm{vol}[V(0)]} \tag{20}$$

for the derivative of the probability that a randomly selected point lies in at least i balls.

Derivative of soft density. Recall the definition of the soft density in (10) and that of the simplified soft density in (11). Accordingly, their derivatives are

$$\frac{\partial \delta_j}{\partial r}(r) = \sum_{i=1}^{j} \frac{\partial \varphi_i}{\partial r}(r) - \sum_{i=j+1}^{\infty} \frac{\partial \varphi_i}{\partial r}(r), \tag{21}$$

$$\frac{\partial \delta_{1\mathrm{s}}}{\partial r}(r) = \sum_{i=1}^{\infty} (3-2i) \frac{\partial \varphi_i}{\partial r}(r) \tag{22}$$

for every integer $j \geq 1$ and every $r \in \mathbb{R}_+$. These derivatives can also be written in terms of areas.

LEMMA 7 (soft density derivative). *Let $j \geq 1$. The derivatives of the jth soft density and of the first simplified soft density of the configuration defined by a lattice $\Lambda \in \mathbb{R}^n$ and a radius $r > 0$ are*

$$\frac{\partial \delta_j}{\partial r}(r) = \frac{2\mathrm{area}[S_j(r)] - \mathrm{area}[\partial B(0,r)]}{\mathrm{vol}[V(0)]}, \tag{23}$$

$$\frac{\partial \delta_{1\mathrm{s}}}{\partial r}(r) = \frac{\mathrm{area}[\partial B(0,r)]}{\mathrm{vol}[V(0)]} - \sum_{0 \neq p \in \Lambda} \frac{2\mathrm{area}[\partial B(0,r) \cap B(p,r)]}{\mathrm{vol}[V(0)]}. \tag{24}$$

Proof. Using (20), we write both sums on the right-hand side of (21) as telescoping sums. Almost all terms cancel, and we get

$$\sum_{i=1}^{j} \frac{\partial \varphi_i}{\partial r}(r) = \frac{\mathrm{area}[S_j(r)]}{\mathrm{vol}[V(0)]}, \tag{25}$$

$$\sum_{i=j+1}^{\infty} \frac{\partial \varphi_i}{\partial r}(r) = \frac{\mathrm{area}[\partial B(0,r)] - \mathrm{area}[S_j(r)]}{\mathrm{vol}[V(0)]}. \tag{26}$$

Subtracting (26) from (25), we get (23). Alternatively, we would start with (12) and get (23) directly. We prefer the latter, geometric argument to prove (24). Indeed, the first term on the right-hand side of (24) is the derivative of the first term on the right-hand side of (13). Similarly, each term in the sum of (24) is the derivative of the corresponding term in the sum of (13). Here we get a factor 2 because

$$\partial[B(0,r) \cap B(p,r)] = [\partial B(0,r) \cap B(p,r)] \cup [B(0,r) \cap \partial B(p,r)]. \tag{27}$$

The two spherical caps on the right-hand side have the same area, so the sum of the areas is twice the area of the first cap. ∎

3.3. Equilibrium. In this subsection, we prove that the soft density of the ball configuration defined by a fixed lattice is a unimodal function of the radius. This property holds for the unsimplified as well as the simplified soft densities.

Fraction versus area. For the proof of unimodality, it will be important that the generalized Voronoi domains centered at 0 are star-convex and contain 0 in the interiors of their kernels; see Lemma 2. To see why this is important, we grow a sphere with center 0. As the radius increases, the fraction of this sphere inside $V_j(0)$ decreases monotonically from 1 to 0. By complementarity, the fraction of the sphere outside $V_j(0)$ increases monotonically from 0 to 1. Plotting the difference between these two fractions as a function of the radius, we get two flat intervals, as seen in

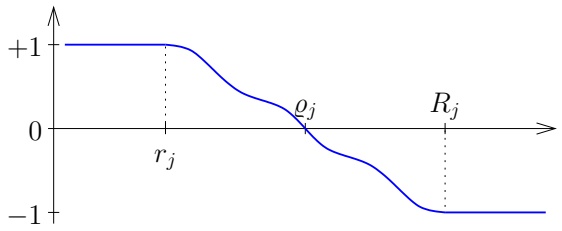

FIG. 4. *The graph of the difference between the fraction of the sphere inside $V_j(0)$ and the complementary fraction outside $V_j(0)$.*

Figure 4, with a monotonically decreasing segment in between. This segment crosses the zero-line exactly once, at the *equilibrium radius*, which we denote by ϱ_j.

Recall that a real-valued function is unimodal if it increases until it attains its maximum, after which it decreases. More formally, we call a differentiable function $f\colon \mathbb{R}_+ \to \mathbb{R}$ *unimodal* if there exists $\varrho \in \mathbb{R}_+$ such that

$$\frac{\partial f}{\partial r}(r) \begin{cases} > 0 & \text{for } r < \varrho, \\ = 0 & \text{for } r = \varrho, \\ < 0 & \text{for } r > \varrho. \end{cases} \tag{28}$$

It follows that the integral of the difference of fractions, as sketched in Figure 4, is unimodal with equilibrium radius ϱ_j. However, according to (23), the derivative of the jth soft density is the difference between the *normalized areas* of the sphere inside and outside $V_j(0)$, and not the difference between the *fractions*.

Unimodality. The jth soft density is unimodal with equilibrium radius ϱ_j nonetheless, but this requires a proof.

LEMMA 8 (unimodality). *Let Λ be a lattice in $\mathbb{R}^n$. For each $j \geq 1$, the jth soft density function of Λ is unimodal, and it attains its maximum at the equilibrium radius of Λ, which satisfies $r_j < \varrho_j < R_j$.*

Proof. We begin by proving that the fraction of the sphere inside the first j rings is monotonically decreasing. Write

$$F(r) = \frac{\text{area}[S_j(r)]}{\text{area}[\partial B(0,r)]} \tag{29}$$

for the fraction, and consider radii $r_j \leq r < R \leq R_j$. Associate each point $x \in \partial B(0,r)$ with the point $y = \frac{R}{r}x \in \partial B(0,R)$. Since $V_j(0)$ is star-convex, with 0 in its kernel, $y \in S_j(R)$ implies that $x \in S_j(r)$. Hence, $F(R) \leq F(r)$. To see that the inequality is strict, we use the fact that 0 lies in the interior of the kernel of $V_j(0)$. We can therefore find a nonempty open arc in $S_j(r)$ such that none of the associated points in $\partial B(0,R)$ belongs to $S_j(R)$. This implies that $F(R) < F(r)$. The difference between the normalized areas inside and outside $V_j(0)$ is

$$\Delta(r) = \frac{2\text{area}[S_j(r)] - \text{area}[\partial B(0,r)]}{\text{vol}[V(0)]} = \frac{\text{area}[\partial B(0,r)]}{\text{vol}[V(0)]} \cdot (2F(r) - 1). \tag{30}$$

This difference has the same sign as $2F(r) - 1$. Hence,

$$\Delta(r) \begin{cases} > 0 & \text{for } r < \varrho_j, \\ = 0 & \text{for } r = \varrho_j, \\ < 0 & \text{for } r > \varrho_j. \end{cases} \tag{31}$$

It follows that δ_j is unimodal and that it attains its maximum at $r = \varrho_j$. We have $r_j < \varrho_j < R_j$ because $2F(r_j) - 1 = 1$ and $2F(R_j) - 1 = -1$. ∎

Remark 1. It is not difficult to adapt the proof of Lemma 8 to show that the following parametrized version of the soft density is also unimodal:

$$\delta_{j,C} = \sum_{i=1}^{j} \varphi_i - \tfrac{1}{C-1} \sum_{i=j+1}^{\infty} \varphi_i, \tag{32}$$

in which $C > 1$ is a constant. Its equilibrium radius is defined by having a fraction of $1/C$ of the sphere inside $V_j(0)$.

Remark 2. The proof of Lemma 8 can also be adapted to show that the first simplified soft density is unimodal. To see that $\delta_{1\mathrm{s}}$ is unimodal, we renormalize by multiplying with $\mathrm{vol}[V(0)]/\mathrm{area}[\partial B(0,r)]$. The first term on the right-hand side of (24) becomes identical 1, and the sum becomes strictly increasing. Hence, there is a unique radius at which the difference vanishes. This is the radius at which $\delta_{1\mathrm{s}}$ attains its maximum.

Counterexamples to unimodality. We have chosen our measures of density carefully so that they are unimodal. Many other choices are not unimodal, and some surprisingly so. Consider, for example, $\pi_i \colon \mathbb{R}_+ \to \mathbb{R}$, defined by mapping r to the probability that a randomly selected point is contained in exactly i balls: $\pi_i = \varphi_i - \varphi_{i+1}$. For lattices in $\mathbb{R}^2$, π_1 is unimodal, and this was exploited in [11] to show that the hexagonal lattice provides the maximizing lattice configuration. But already in $\mathbb{R}^3$, π_1 is not necessarily unimodal, as we now show. Let

$$a_1 = \begin{bmatrix} 1 \\ 0 \\ 0 \end{bmatrix}, \; a_2 = \begin{bmatrix} 0 \\ 4 \\ 0 \end{bmatrix}, \; a_3 = \begin{bmatrix} 0 \\ 0 \\ 4 \end{bmatrix}. \tag{33}$$

The packing radius of the thus defined lattice $\Lambda \subseteq \mathbb{R}^3$ is 0.5. Increasing the radius from 0.0 to 1.0, the probability grows monotonically from $\pi_1(0.0) = 0$ to $\pi_1(1.0) = \frac{\pi}{2}$. Let $D_*(r)$ be the set of points in $B(0,r)$ that are not contained in any other balls. The boundary of $D_*(r)$ consists of points on $\partial B(0,r)$ and of points on other spheres in the configuration. We then write $\partial D_*(r) = S_0(r) \cup S(r)$, with $S_0(r) \subseteq \partial B(0,r)$ and $S(r) \subseteq B(0,r) \setminus \partial B(0,r)$; see Figure 5. For $r = 1.0$, Archimedes' theorem implies that the two have the same area. Writing $f(r) = \mathrm{vol}[D_*(r)]$, the derivative vanishes:

$$\frac{\partial f}{\partial r}(1.0) = \mathrm{area}[S_0(1.0)] - \mathrm{area}[S(1.0)] = 0. \tag{34}$$

Indeed, if we increase r moderately beyond 1.0, we keep getting constant volume and vanishing derivative. More precisely, we get $f(r) = \frac{\pi}{2}$ for $1.0 \leq r \leq 2.0$, with smaller values for all other radii. In summary, $\pi_1(r) = f(r)/\mathrm{vol}[V(0)]$ has an interval of maxima, which contradicts unimodality.

Extending this example to four and higher dimensions, it is possible to get functions $\pi_1 \colon \mathbb{R}_+ \to \mathbb{R}$ with multiple local maxima separated from each other by valleys of lower probability.

4. Optimality in $\mathbb{R}^3$. This section presents the case analysis we use to prove Theorem 1 stated in the introduction. As a warm-up exercise, we compute the first soft density of the equilibrium configurations of the FCC lattice in $\mathbb{R}^3$.

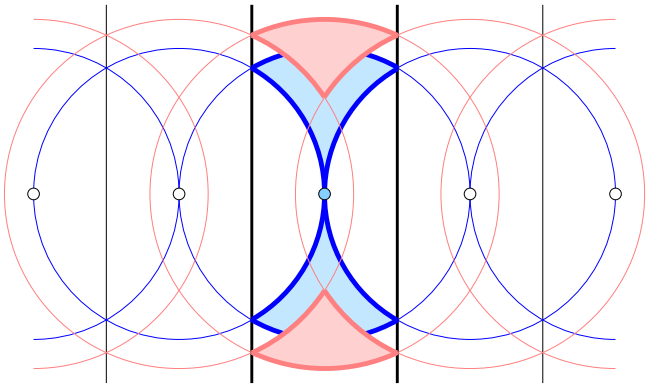

FIG. 5. *Front view of a row of unit spheres and, superimposed, of the same row of slightly enlarged spheres. The shaded sets $D_*(r)$ are contained in the first Voronoi domain of* 0.

FCC lattice. We generate the face centered cubic lattice with the vectors

$$a_1 = \begin{bmatrix} 4/3 \\ 1/3 \\ 1/3 \end{bmatrix}, \; a_2 = \begin{bmatrix} 1/3 \\ 4/3 \\ 1/3 \end{bmatrix}, \; a_3 = \begin{bmatrix} 1/3 \\ 1/3 \\ 4/3 \end{bmatrix}. \tag{35}$$

The packing radius is half the minimum distance between the points, which is $r = \frac{\sqrt{2}}{2}$. The volume of the Voronoi domain is also the volume of the parallelepiped spanned by the generating vectors:

$$\text{vol}[V(0)] = \det \begin{bmatrix} 4/3 & 1/3 & 1/3 \\ 1/3 & 4/3 & 1/3 \\ 1/3 & 1/3 & 4/3 \end{bmatrix} = 2. \tag{36}$$

The equilibrium radius is $\varrho = \frac{12}{11} r = \frac{6\sqrt{2}}{11}$. Indeed, at this radius a sphere intersects the neighboring balls in 12 equal and nonintersecting caps, each $\frac{1}{24}$ of the area of the sphere. The caps are in the direction of the vectors $\pm a_i$ and $a_i - a_j$, for $i, j \in \{1, 2, 3\}$, and have area

$$\text{A}_{\text{Cap}} = 2\pi\varrho(\varrho - r) = \tfrac{24\pi r^2}{11^2} = 0.311\ldots. \tag{37}$$

The volume of a ball is

$$\text{V}_{\text{Ball}} = \text{vol}[B(0, \varrho)] = \tfrac{4\pi}{3}\varrho^3 = \tfrac{16 \cdot 12^2 \pi r^3}{11^3} = 1.922\ldots. \tag{38}$$

The volume of the cone over a cap is $\frac{1}{24}$ of this. The boundary of the cap is a circle which spans a disk, and the volume of the cone over this disk is

$$\text{V}_{\text{Cone}} = (\varrho^2 - r^2)\tfrac{r\pi}{3} = \tfrac{23\pi r^3}{3 \cdot 11^2} = 0.070\ldots. \tag{39}$$

Referring to the difference between a cone over the cap and the cone over the disk as a segment of the ball, we note that its volume is $\text{V}_{\text{Sgmt}} = \frac{1}{24}\text{V}_{\text{Ball}} - \text{V}_{\text{Cone}}$. To finally compute the first soft density, we get φ_1 as the normalized volume of the ball minus 12 segments, φ_2 as the normalized volume of 12 segments, and the first soft density

as the difference:

$$\varphi_1 = \tfrac{1}{2}(\tfrac{1}{2}\mathrm{V}_{\mathrm{Ball}} + 12\mathrm{V}_{\mathrm{Cone}}) = \tfrac{1082\pi r^3}{11^3} = \tfrac{541\sqrt{2}\pi}{2\cdot 11^3} = 0.902\ldots, \tag{40}$$

$$\varphi_2 = \tfrac{1}{2}(\tfrac{1}{2}\mathrm{V}_{\mathrm{Ball}} - 12\mathrm{V}_{\mathrm{Cone}}) = \tfrac{70\pi r^3}{11^3} = \tfrac{35\sqrt{2}\pi}{2\cdot 11^3} = 0.058\ldots, \tag{41}$$

$$\delta_1 = \varphi_1 - \varphi_2 = \tfrac{92\pi r^3}{11^2} = \tfrac{23\sqrt{2}\pi}{11^2} = 0.844\ldots. \tag{42}$$

Since there are no triple intersections, this is also the first simplified soft density: $\delta_1 = \delta_{1\mathrm{s}}$. By comparison, the first soft density of the BCC lattice is $0.832\ldots$.

1-*parameter family of lattices.* We consider the *diagonal family* of lattices introduced in [12]. Each lattice in this family is obtained by compressing or stretching the integer lattice, $\mathbb{Z}^3$, along the diagonal direction. Writing u_1, u_2, u_3 for the unit coordinate vectors, which span $\mathbb{Z}^3$, and $\mathbf{1} = u_1 + u_2 + u_3$, we define

$$u_i(\varepsilon) = u_i + \tfrac{\varepsilon-1}{3}\cdot\mathbf{1}, \tag{43}$$

for $1 \le i \le 3$, and we let Λ_ε be the lattice generated by these vectors. Note that $\langle u_i(\varepsilon), \mathbf{1}\rangle = 1 + (\varepsilon - 1)$, which shows that for $\varepsilon = 0$, all three vectors are orthogonal to $\mathbf{1}$ and therefore not linearly independent. We get a lattice for every $\varepsilon > 0$, and particularly interesting examples are the BCC lattice at $\varepsilon = \frac{1}{2}$, the integer lattice at $\varepsilon = 1$, and the FCC lattice at $\varepsilon = 2$.

For $\varepsilon = 1$, the Voronoi domain is the unit cube, $V(0) = [-\frac{1}{2}, \frac{1}{2}]^3$, which has volume 1. More generally, the Voronoi domain of Λ_ε has volume ε, namely the same volume as the parallelotope defined by $u_1(\varepsilon)$, $u_2(\varepsilon)$, $u_3(\varepsilon)$. As observed already in [13], the Voronoi domains for parameters $0 < \varepsilon < 1$ are all combinatorially equivalent, being bounded by eight hexagons and six rectangles. Similarly, the Voronoi domains for $1 < \varepsilon < \infty$ are combinatorially equivalent, being bounded by 12 rhombi; see Figure 6. This combinatorial predictability of the Voronoi domain enables the detailed analyses in [12, 18] as well as in this paper. Given a value of the parameter ε and a radius r, we need to determine which faces, edges, and vertices of $V(0)$ intersect $B(0, r)$. Fixing ε, we call r a *critical radius* if there is a face, edge, or vertex of $V(0)$ that touches $B(0, r)$ but is disjoint of its interior. Because of the symmetry of the configuration, there are very few critical radii. For $0 < \varepsilon < 1$, these have already been determined

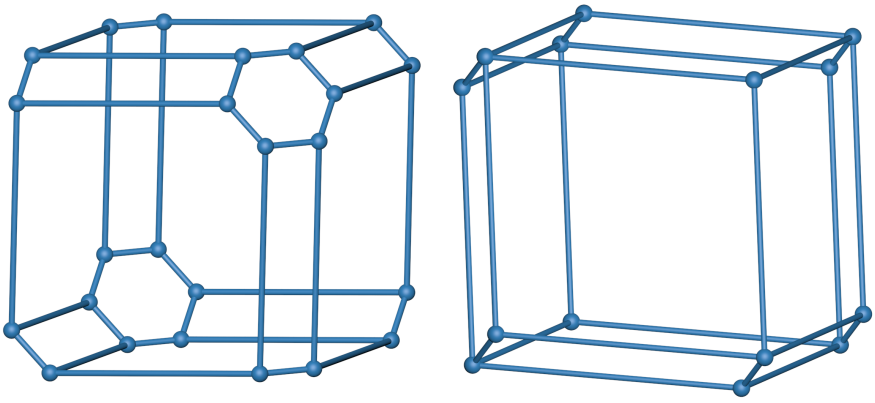

FIG. 6. *The Voronoi domains of* Λ_ε *for* ε *slightly smaller than* 1 *on the* left *and for* ε *slightly larger than* 1 *on the* right.

in [18]. With reference to Figure 6, they are

$$f_1(\varepsilon) = \sqrt{(\varepsilon^2+2)/12}, \tag{44}$$

$$f_2(\varepsilon) = \sqrt{(2\varepsilon^2+1)/6}, \tag{45}$$

$$f_3(\varepsilon) = \sqrt{3}\varepsilon/2, \tag{46}$$

$$e_1(\varepsilon) = (\varepsilon^2+2)/(3\sqrt{2}), \tag{47}$$

$$e_2(\varepsilon) = \sqrt{(\varepsilon^2+2)(2\varepsilon^2+1)}/(2\sqrt{3}), \tag{48}$$

$$v_1(\varepsilon) = \sqrt{8\varepsilon^4+11\varepsilon^2+8}/6, \tag{49}$$

corresponding to the six square-like hexagons, six rectangles, two small hexagons, 18 long edges, 18 short edges, and 24 vertices of the polytope on the left in Figure 6. Similarly, for $1 < \varepsilon < \infty$, we have six critical radii:

$$f_1(\varepsilon) = \sqrt{(\varepsilon^2+2)/12}, \tag{50}$$

$$f_4(\varepsilon) = \sqrt{2}/2, \tag{51}$$

$$e_3(\varepsilon) = \sqrt{6}/3, \tag{52}$$

$$e_4(\varepsilon) = (\varepsilon^2+2)/\sqrt{12\varepsilon^2+6}, \tag{53}$$

$$v_2(\varepsilon) = (\varepsilon^2+2)/(2\sqrt{3}\varepsilon), \tag{54}$$

$$v_3(\varepsilon) = \sqrt{\varepsilon^2+8}/(2\sqrt{3}), \tag{55}$$

corresponding to the six square-like rhombi, six narrow rhombi, six short edges, 18 long edges, eight degree-3 vertices, and six degree-4 vertices of the polytope on the right in Figure 6. See Appendix A.1 for details.

Soft density at equilibrium. Given a lattice Λ_ε in the diagonal family, we write $\delta_1(\varepsilon) = \max_{r>0} \delta_1(\Lambda_\varepsilon, r)$ for the maximum soft density and $\delta_{1\mathrm{s}}(\varepsilon) = \max_{r>0} \delta_{1\mathrm{s}}(\Lambda_\varepsilon, r)$ for the maximum simplified soft density. As argued in the preceding sections, the maxima are obtained for the respective equilibrium radii. To compute the maximum soft density of every lattice Λ_ε, we divide $\mathbb{R}_+$ into 12 intervals such that within every interval the expressions and the order of the critical and equilibrium radii are constant. Table 1 summarizes the pertinent information for all 12 intervals. Note that in Cases I–IX, the equilibrium radius precedes the critical radii that belong to edges and vertices of the Voronoi domains. Equivalently, the equilibrium configuration contains pairwise but no triplewise overlaps among the balls. In these cases, the soft density equals the simplified soft density: $\delta_1(\varepsilon) = \delta_{1\mathrm{s}}(\varepsilon)$. Indeed, we do all computations for the simplified soft density, which by construction considers only pairwise intersections, and we will find that the FCC lattice maximizes this measure. The equilibrium configuration has triple intersections only for lattices with values of ε larger than that of the FCC lattice, and to prove that the FCC lattice also maximizes the unsimplified soft density, we will finally bound the soft density of these equilibrium configurations from above. To do the computations for the simplified density, we determine the number and type of the spherical caps, and we determine the equilibrium radius, $\varrho = \varrho_1$, at which these caps amount to half the surface area. Note that the number and type of caps is the same in Cases II and III, in Cases IV–VII, and—because we ignore triple overlaps for the time being—in Cases VIII–XI. The 12 cases thus consolidate to five, which we discuss in sequence.

Case I. Here we have two caps, both with critical radius $f_3(\varepsilon)$. At the equilibrium radius, each of the caps covers one quarter of the sphere. Accordingly, the equilibrium

TABLE 1

The order of the equilibrium radius among the critical radii. Within each of the 12 *intervals dividing the positive number line, the order is independent of the parameter* ε. *Precise expressions for the interval endpoints can be found in Appendix* A.

Case	Critical and equilibrium radii	Interval
I	$f_3 \le \varrho \le f_1 \le f_2 \le e_2 \le e_1 \le v_1$	$(0.000\ldots, 0.239\ldots]$
II	$f_3 \le f_1 \le \varrho \le f_2 \le e_2 \le e_1 \le v_1$	$[0.239\ldots, 0.500\ldots]$
III	$f_1 \le f_3 \le \varrho \le f_2 \le e_1 \le e_2 \le v_1$	$[0.500\ldots, 0.617\ldots]$
IV	$f_1 \le \varrho \le f_3 \le f_2 \le e_1 \le e_2 \le v_1$	$[0.617\ldots, 0.632\ldots]$
V	$f_1 \le \varrho \le f_2 \le f_3 \le e_1 \le e_2 \le v_1$	$[0.632\ldots, 0.664\ldots]$
VI	$f_1 \le \varrho \le f_2 \le e_1 \le f_3 \le e_2 \le v_1$	$[0.664\ldots, 1.000\ldots]$
VII	$f_1 \le \varrho \le f_4 \le e_4 \le e_3 \le v_2 \le v_3$	$[1.000\ldots, 1.471\ldots]$
VIII	$f_1 \le f_4 \le \varrho \le e_4 \le e_3 \le v_2 \le v_3$	$[1.471\ldots, 2.000\ldots]$
IX	$f_4 \le f_1 \le \varrho \le e_3 \le e_4 \le v_2 \le v_3$	$[2.000\ldots, 2.342\ldots]$
X	$f_4 \le f_1 \le e_3 \le \varrho \le e_4 \le v_2 \le v_3$	$[2.342\ldots, 2.449\ldots]$
XI	$f_4 \le e_3 \le f_1 \le \varrho \le e_4 \le v_2 \le v_3$	$[2.449\ldots, 2.576\ldots]$
XII	$f_4 \le e_3 \le \varrho \le f_1 \le e_4 \le v_2 \le v_3$	$[2.576\ldots, \infty)$

radius and the soft density are

$$\varrho(\varepsilon) = \sqrt{3}\varepsilon, \tag{56}$$

$$\delta_1(\varepsilon) = \delta_{1s}(\varepsilon) = 3\sqrt{3}\pi\varepsilon^2/2. \tag{57}$$

The derivative of δ_1 is positive in the entire interval, as can be seen in Figure 7.

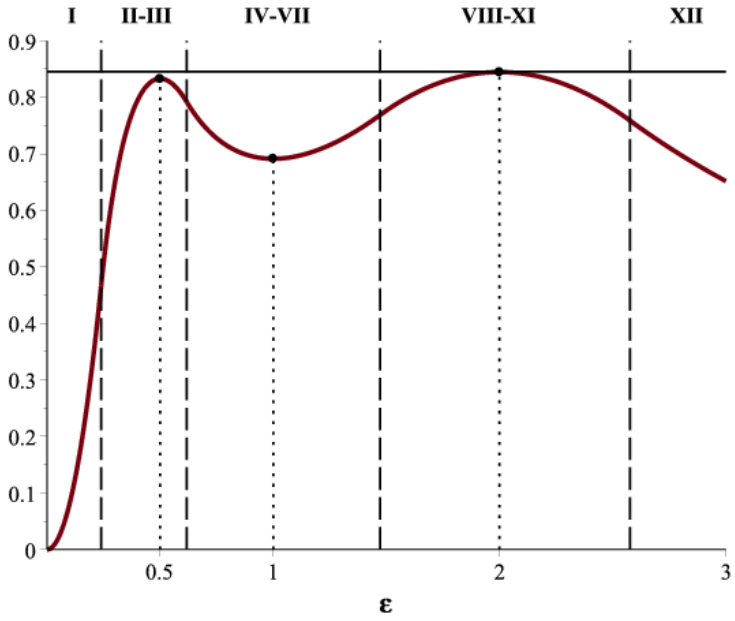

FIG. 7. *The graph of the maximum simplified soft density,* δ_{1s}, *as a function of* ε, *which parametrizes the lattices in the diagonal family. From* 0 *to* $2.342\ldots$, *this is identical to the graph of the maximum soft density,* δ_1.

Cases II *and* III. Here we have eight caps, two with critical radius $f_3(\varepsilon)$ and six with critical radius $f_1(\varepsilon)$. At the equilibrium, these caps cover half the sphere. The

equilibrium radius and the corresponding soft density are

$$\varrho(\varepsilon) = \tfrac{\varepsilon\sqrt{3}+\sqrt{3\varepsilon^2+6}}{7}, \tag{58}$$

$$\delta_1(\varepsilon) = \delta_{1\mathrm{s}}(\varepsilon) = \tfrac{\pi[27\sqrt{3}\varepsilon(11\varepsilon^2-8)+(26-95\varepsilon^2)\sqrt{3\varepsilon^2+6}]}{882\varepsilon}. \tag{59}$$

The derivative vanishes at $\varepsilon = \frac{1}{2}$, and the second derivative is negative throughout the entire open interval. It follows that δ_1 is concave over the interval, with maximum at $\varepsilon = \frac{1}{2}$, which corresponds to the BCC lattice; see Figure 7.

Cases IV–VII. Here we have six caps, all with critical radius $f_1(\varepsilon)$. The corresponding equilibrium radius and the corresponding soft density are

$$\varrho(\varepsilon) = \tfrac{\sqrt{3\varepsilon^2+6}}{5}, \tag{60}$$

$$\delta_1(\varepsilon) = \delta_{1\mathrm{s}}(\varepsilon) = \tfrac{11\pi\sqrt{(3\varepsilon^2+6)^3}}{1350\varepsilon}. \tag{61}$$

The derivative vanishes at $\varepsilon = 1$, and the second derivative is positive throughout the entire open interval. It follows that δ_1 is convex over the interval, with minimum at $\varepsilon = 1$, which corresponds to the integer lattice; see Figure 7.

Cases VIII–XI. Here we have 12 caps, six each with critical radii $f_1(\varepsilon)$ and $f_4(\varepsilon)$. Ignoring intersections among these caps, we compute the equilibrium radius such that the total area of the 12 caps equals half the sphere. The equilibrium radius and the corresponding simplified soft density are

$$\varrho(\varepsilon) = \tfrac{\sqrt{3\varepsilon^2+6}+3\sqrt{2}}{11}, \tag{62}$$

$$\delta_{1\mathrm{s}}(\varepsilon) = \tfrac{\pi[324\sqrt{2}\varepsilon^2-882\sqrt{2}+(478-85\varepsilon^2)\sqrt{3\varepsilon^2+6}]}{2178\varepsilon}. \tag{63}$$

The derivative vanishes at $\varepsilon = 2$, and the second derivative is negative throughout the entire open interval. It follows that δ_1 is concave, with maximum at $\varepsilon = 2$, which corresponds to the FCC lattice; see Figure 7.

Case XII. Here we have six caps, all with critical radius $f_4(\varepsilon)$. Ignoring intersections among these caps, the equilibrium radius and the corresponding simplified soft density are

$$\varrho(\varepsilon) = \tfrac{3\sqrt{2}}{5}, \tag{64}$$

$$\delta_{1\mathrm{s}}(\varepsilon) = \tfrac{11\sqrt{2}\pi}{25\varepsilon}. \tag{65}$$

The derivative of $\delta_{1\mathrm{s}}$ is negative throughout the interval.

The above case analysis is summarized in Figure 7, which shows the maximum simplified soft density as a function of ε. We see that there are two local maxima separated by a local minimum, with

$$\delta_{1\mathrm{s}}(0.5) = 0.832\ldots, \tag{66}$$

$$\delta_{1\mathrm{s}}(1.0) = 0.691\ldots, \tag{67}$$

$$\delta_{1\mathrm{s}}(2.0) = 0.844\ldots, \tag{68}$$

corresponding to the BCC, the integer, and the FCC lattices, all members of the diagonal family. For $\varepsilon < 2.342\ldots$, the maximum is achieved without triple intersections, which implies that $\delta_1(\varepsilon) = \delta_{1\mathrm{s}}(\varepsilon)$. In particular, (66), (67), (68) remain valid after substituting δ_1 for $\delta_{1\mathrm{s}}$. This is consistent with Theorem 1, which claims that the FCC lattice maximizes the soft density, but it is not yet quite a proof. Indeed, we still need information on the behavior of δ_1 for $\varepsilon > 2.342\ldots$. We will now fill this gap and thus complete the proof of Theorem 1. The main new idea is another measure of density, which we will show majorizes the maximum soft density.

Extrapolated soft density. Consider the FCC lattice, at $\varepsilon = 2$, as described at the beginning of this section. At the equilibrium, the ball centered at the origin intersects 12 other balls whose centers lie in three planes. Specifically, three of the 12 centers satisfy $\langle p, \mathbf{1}\rangle = -2$, six centers satisfy $\langle p, \mathbf{1}\rangle = 0$, and three centers satisfy $\langle p, \mathbf{1}\rangle = 2$. As ε increases, these three planes move apart until the ball at 0 intersects only the six balls in the middle plane at equilibrium. For the simplified soft density, this happens for $\varepsilon > 2.576\ldots$, and for the unsimplified soft density it happens a little later, for $\varepsilon > 2.62\ldots$. Within a plane orthogonal to the diagonal, the lattice points do not move, which implies that for all ε larger than some threshold, all equilibrium configurations are the same: a ball surrounded by six others forming a regular hexagon around 0. This corresponds to Case XII. It follows that for each radius r, there are a threshold $\varepsilon_0(r)$ and a constant $C(r)$, such that the soft density has the form

$$\delta_1(\Lambda_\varepsilon, r) = \tfrac{C(r)}{\varepsilon} \tag{69}$$

for all $\varepsilon > \varepsilon_0(r)$. Similarly, the equilibrium radius remains constant beyond this threshold, and the maximum soft density satisfies $\delta_1(\varepsilon) = C/\varepsilon$, in which $C = C(\varrho(\varepsilon))$ for large enough ε. Since we define the constant for the unsimplified soft density, it is slightly larger than it would be for the simplified soft density given in (65), namely $1.96 > 1.95 \approx 11\sqrt{2}\pi/25$; see Appendix A.4 for details. We define the *extrapolated soft density* as

$$\delta_{1\mathrm{x}}(\Lambda_\varepsilon, r) = \tfrac{C(r)}{\varepsilon}, \tag{70}$$

but now for all $\varepsilon > 0$. Similarly, $\delta_{1\mathrm{x}}(\varepsilon) = C/\varepsilon$ is the maximum extrapolated soft density. While we define $\delta_{1\mathrm{x}}$ for all positive ε, we are really only interested in $\varepsilon \geq 2.342\ldots$—the range in which the equilibrium configuration contains triple intersections among the balls. At that parameter value, we have $\delta_{1\mathrm{x}}(2.342\ldots) = 1.96\ldots/2.342\ldots = 0.837\ldots$, which is smaller than $\delta_1(2) = 0.844\ldots$; see Appendix A.4 for the details necessary to see that this inequality is preserved if we use the precise numbers.

Majorization. It remains to prove that the maximum extrapolated soft density majorizes the maximum soft density, which in turn majorizes the maximum simplified soft density.

LEMMA 9 (majorization). *We have*

$$\delta_{1\mathrm{s}}(\varepsilon) \leq \delta_1(\varepsilon) \leq \delta_{1\mathrm{x}}(\varepsilon) \tag{71}$$

for all $\varepsilon > 0$.

Proof. We first prove the left inequality. Recall from (10) and (11) that for a given lattice and a given radius, we have

$$\delta_1(\Lambda, r) = \varphi_1 - \varphi_2 - \varphi_3 - \varphi_4 - \cdots, \tag{72}$$

$$\delta_{1\mathrm{s}}(\Lambda, r) = \varphi_1 - \varphi_2 - 3\varphi_3 - 5\varphi_4 - \cdots. \tag{73}$$

This implies that $\delta_{1\mathrm{s}}(\Lambda, r) \leq \delta_1(\Lambda, r)$ for all lattices and all radii. To extend this inequality to the corresponding maxima, we write $\varrho_{1\mathrm{s}}$ for the equilibrium radius of Λ_ε under the simplified soft density. Then

$$\delta_{1\mathrm{s}}(\varepsilon) = \delta_{1\mathrm{s}}(\Lambda_\varepsilon, \varrho_{1\mathrm{s}}) \leq \delta_1(\Lambda_\varepsilon, \varrho_{1\mathrm{s}}) \leq \delta_1(\varepsilon), \tag{74}$$

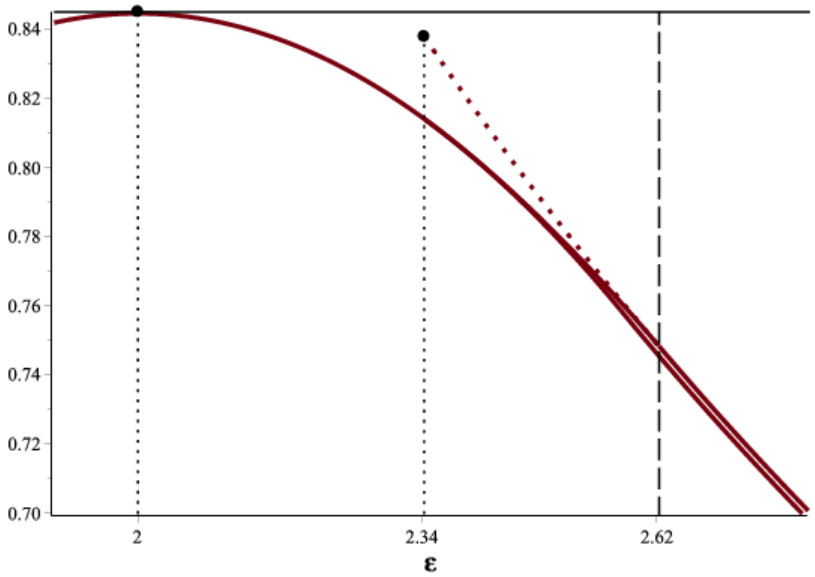

FIG. 8. *A part of the simplified soft density function, with maximum at* $\varepsilon = 2$. *On the right and slightly above the graph of* δ_{1s}, *we see the graph of the soft density function,* δ_1, *with the dotted extrapolated portion ending at the point* $(2.342\ldots, 0.837\ldots)$.

in which the last inequality follows by definition of $\delta_1(\varepsilon)$ as the maximum soft density of Λ_ε.

Seond, we prove the right inequality. For a given lattice, Λ_ε, and a given radius, r, we have $\delta_1(\Lambda_\varepsilon, r) \leq \delta_{1x}(\Lambda_\varepsilon, r)$, simply because the latter accounts for a subset of the balls that enter the computation of the soft density. Now let $\varrho_1 = \varrho_1(\varepsilon)$ be the equilibrium radius of Λ_ε under the soft density. Then

$$\delta_1(\varepsilon) = \delta_1(\Lambda_\varepsilon, \varrho_1) \leq \delta_{1x}(\Lambda_\varepsilon, \varrho_1) \leq \delta_{1x}(\varepsilon), \tag{75}$$

in which the last inequality follows by the definition of $\delta_{1x}(\varepsilon)$ as the maximum extrapolated soft density of Λ_ε. ∎

The two inequalities are illustrated in Figure 8. Together with $\delta_{1x}(2.342\ldots) < \delta_1(2)$, they imply that the FCC lattice at $\varepsilon = 2$ is the unique maximum of δ_1 over the entire diagonal family of lattices. This completes the proof of Theorem 1.

5. Discussion. The main contributions of this paper are the definition of soft density of a lattice sphere configuration and the proof that among the 3-dimensional lattices in the diagonal family introduced in [12], the first soft density is maximized at the FCC lattice. A key step in the proof of optimality is the unimodality of the soft density for any given lattice. Indeed, unimodality holds for all $j \geq 1$ and all dimensions $n \geq 1$.

Optimal lattices. A difficult question is the determination of the lattices that maximize the jth soft density. For $j = 1$ and $n = 2$ dimensions, the optimal configuration has been determined in [1], but for $j \geq 2$, we do not have a proof that the hexagonal lattice provides the optimum. In $n = 3$ dimensions, there are no results beyond what we proved in this paper, namely that the FCC lattice gives the optimum among the lattices in the diagonal family introduced in [12]:

- Does the FCC lattice give the maximum first soft density among all lattices in $\mathbb{R}^3$?
- What about values of j larger than 1 and dimensions n larger than 3?
- Does the FCC lattice maximize the probability that a random point belongs to exactly one ball of the configuration?

Short of proving that the FCC lattice maximizes δ_1 among all lattices in $\mathbb{R}^3$, it might be possible to use Csikós' formula for the volume derivative [8] to at least show that the FCC lattice furnishes a local maximum.

Nonlattice configurations. The notion of soft density can be extended to nonlattice configurations of balls: within a region $\Omega \subseteq \mathbb{R}^n$, we compute the probability, φ_i, that a randomly selected point belongs to at least i balls, we set $\delta_j = \varphi_1 + \cdots + \varphi_j - \varphi_{j+1} - \cdots$, we increase Ω, and we finally take the limit. Fixing the centers and growing the balls, we again get a function of the radius, but it is not necessarily unimodal. Indeed, we can define the generalized Voronoi domains of a point p in the configuration as before. Extending Lemma 6 and using the star-convexity of the $V_j(p)$, we can show that the difference between the volume of $B(p, r)$ inside and outside $V_j(p)$ is a unimodal function of r. However, the sum of these unimodal functions over different points in the configuration is not necessarily unimodal. This lack of global unimodality is likely to make progress on soft packing for nonlattice configurations difficult to come by.

Appendix A. Case analysis. In this appendix, we present the computations needed to determine the maximum soft density as a function of ε, which parametrizes the lattices in the diagonal family. We begin with describing the critical radii of the faces of the Voronoi polytope and continue with finding the positions of the equilibrium radii among the critical radii.

A.1. Critical radii. The critical radii listed in section 4 correspond to the radii at which a growing ball centered at the origin touches different faces of the Voronoi domain; see Table 2. For $\varepsilon \leq 1$, f_1 corresponds to the six square-like hexagons normal to the $\pm u_i(\varepsilon)$, f_2 to the six rectangles normal to the $\pm[u_i(\varepsilon) + u_j(\varepsilon)]$, f_3 to the two small hexagons normal to $\pm[u_1(\varepsilon) + u_2(\varepsilon) + u_3(\varepsilon)]$, e_1 to the 18 long edges parallel to the vectors $u_i(\varepsilon) \times u_j(\varepsilon)$, e_2 to the 18 short edges parallel to the vectors $u_i(\varepsilon) \times [u_1(\varepsilon) + u_2(\varepsilon) + u_3(\varepsilon)]$, and the covering radius, v_1, corresponding to the 24 vertices of the polytope on the left in Figure 6. For $\varepsilon \geq 1$, f_1 corresponds to the six square-like rhombi normal to the $\pm u_i(\varepsilon)$, f_4 to the six narrow rhombi normal to the $u_i(\varepsilon) - u_j(\varepsilon)$, e_3 to the six short edges parallel to the vectors $[u_i(\varepsilon) - u_j(\varepsilon)] \times [u_i(\varepsilon) - u_k(\varepsilon)]$ or, equivalently, parallel to the vector $u_1(\varepsilon) + u_2(\varepsilon) + u_3(\varepsilon)$, e_4 to the 18 long edges parallel to the vectors $u_i(\varepsilon) \times u_j(\varepsilon)$, v_2 to the eight degree-3 vertices, and the covering radius, v_3, corresponding to the six degree-4 vertices of the polytope on the right in Figure 6 for $i, j \in \{1, 2, 3\}$ and $\ell, m \in \{2, 3\}$.

After ordering the critical radii, we are left with seven sequences, which we show in Table 3.

A.2. Position of equilibrium radius. Given a constant ordering of the critical radii over an interval of values ε, we find the equilibrium radius by searching in this sequence. At any one step, we consider a particular critical radius, and we compute the area of the sphere covered by the corresponding caps. If this is more than half of the sphere, then the search continues on the left, and if it is less than half, then the search continues on the right. It is also possible that it switches from more to less than half within the interval, in which case we divide the interval and search in the subintervals independently.

TABLE 2

The right column gives the centers of the spheres that define the corresponding critical radius, namely the minimum radius at which these spheres have a nonempty common intersection. Notice that although at radius v_3 only eight vertices are met, they correspond to the circumcenter of 16 *tetrahedra around the origin.*

Radius	Value	Vectors
$f_1(\varepsilon)$	$\sqrt{(\varepsilon^2+2)/12}$	$[0, \pm u_i(\varepsilon)]$
$f_2(\varepsilon)$	$\sqrt{(2\varepsilon^2+1)/6}$	$\pm[0, u_i(\varepsilon) + u_j(\varepsilon)]$
$f_3(\varepsilon)$	$\sqrt{3}\varepsilon/2$	$\pm[0, \mathbf{1}(\varepsilon)]$
$e_1(\varepsilon)$	$(\varepsilon^2+2)/(3\sqrt{2})$	$[0, u_i(\varepsilon), -u_j(\varepsilon)]$ $\pm[0, u_i(\varepsilon), u_i(\varepsilon) + u_j(\varepsilon)]$
$e_2(\varepsilon)$	$\sqrt{(\varepsilon^2+2)(2\varepsilon^2+1)}/(2\sqrt{3})$	$\pm[0, \mathbf{1}(\varepsilon), u_i(\varepsilon)]$ $\pm[0, \mathbf{1}(\varepsilon), u_i(\varepsilon) + u_j(\varepsilon)]$ $\pm[0, -u_i(\varepsilon), u_j(\varepsilon) + u_k(\varepsilon)]$
$v_1(\varepsilon)$	$\sqrt{8\varepsilon^4+11\varepsilon^2+8}/6$	$\pm[0, \mathbf{1}(\varepsilon), u_i(\varepsilon), u_i(\varepsilon) + u_j(\varepsilon)]$ $\pm[0, -u_i(\varepsilon), u_j(\varepsilon) + u_k, u_j(\varepsilon)]$
$f_4(\varepsilon)$	$\sqrt{2}/2$	$u_i(\varepsilon) - u_j(\varepsilon)$
$e_3(\varepsilon)$	$\sqrt{6}/3$	$\pm[0, u_i(\varepsilon) - u_j(\varepsilon), u_i(\varepsilon) - u_k(\varepsilon)]$
$e_4(\varepsilon)$	$(\varepsilon^2+2)/\sqrt{12\varepsilon^2+6}$	$\pm[0, u_i(\varepsilon), u_j(\varepsilon)]$ $\pm[0, u_i(\varepsilon), u_i(\varepsilon) - u_j(\varepsilon)]$
$v_2(\varepsilon)$	$(\varepsilon^2+2)/(2\sqrt{3}\varepsilon)$	$\pm[0, u_1(\varepsilon), u_2(\varepsilon), u_3(\varepsilon)]$ $\pm[0, u_i(\varepsilon), u_i(\varepsilon) - u_j(\varepsilon), u_i(\varepsilon) - u_k(\varepsilon)]$
$v_3(\varepsilon)$	$\sqrt{\varepsilon^2+8}/(2\sqrt{3})$	$\pm[0, u_\ell(\varepsilon), u_1(\varepsilon) - u_m(\varepsilon), u_1]$ $\pm[0, u_\ell(\varepsilon), u_1(\varepsilon) - u_m(\varepsilon), u_\ell(\varepsilon) - u_m(\varepsilon)]$ $\pm[0, u_\ell(\varepsilon) + u_m(\varepsilon) - u_1, u_\ell(\varepsilon), u_m(\varepsilon)]$ $\pm[0, u_\ell(\varepsilon) + u_m(\varepsilon) - u_1, u_\ell(\varepsilon), u_\ell(\varepsilon) - u_1(\varepsilon)]$ $\pm[0, u_\ell(\varepsilon) + u_m(\varepsilon) - u_1, u_\ell(\varepsilon) - u_1(\varepsilon), u_m(\varepsilon) - u_1(\varepsilon)]$

TABLE 3

Sequences of critical radii.

Ordering	Interval
$f_3(\varepsilon) \le f_1(\varepsilon) \le f_2(\varepsilon) \le e_2(\varepsilon) \le e_1(\varepsilon) \le v_1(\varepsilon)$	$0.000\ldots \le \varepsilon \le 0.500\ldots$
$f_1(\varepsilon) \le f_3(\varepsilon) \le f_2(\varepsilon) \le e_1(\varepsilon) \le e_2(\varepsilon) \le v_1(\varepsilon)$	$0.500\ldots \le \varepsilon \le 0.632\ldots$
$f_1(\varepsilon) \le f_2(\varepsilon) \le f_3(\varepsilon) \le e_1(\varepsilon) \le e_2(\varepsilon) \le v_1(\varepsilon)$	$0.632\ldots \le \varepsilon \le 0.664\ldots$
$f_1(\varepsilon) \le f_2(\varepsilon) \le e_1(\varepsilon) \le f_3(\varepsilon) \le e_2(\varepsilon) \le v_1(\varepsilon)$	$0.664\ldots \le \varepsilon \le 1.000\ldots$
$f_1(\varepsilon) \le f_4(\varepsilon) \le e_4(\varepsilon) \le e_3(\varepsilon) \le v_2(\varepsilon) \le v_3(\varepsilon)$	$1.000\ldots \le \varepsilon \le 2.000\ldots$
$f_4(\varepsilon) \le f_1(\varepsilon) \le e_3(\varepsilon) \le e_4(\varepsilon) \le v_2(\varepsilon) \le v_3(\varepsilon)$	$2.000\ldots \le \varepsilon \le 2.449\ldots$
$f_4(\varepsilon) \le e_3(\varepsilon) \le f_1(\varepsilon) \le e_4(\varepsilon) \le v_2(\varepsilon) \le v_3(\varepsilon)$	$2.449\ldots \le \varepsilon$

First sequence. Referring to the first two rows in Table 1, we note that for $0 < \varepsilon \le 0.5$, the sorted sequence of critical radii is $f_3(\varepsilon) \le f_1(\varepsilon) \le f_2(\varepsilon) \le e_2(\varepsilon) \le e_1(\varepsilon) \le v_1(\varepsilon)$. Recall that the first critical radius is the packing radius and thus precedes the equilibrium radius in all cases. We begin the search by testing the second critical radius. At radius $f_1(\varepsilon)$, the ball intersects two facets of the Voronoi domain, both at distance $f_3(\varepsilon)$ from the origin. We therefore get two caps, and using (44) and (46), we get their height and area as

$$h(\varepsilon) = f_1(\varepsilon) - f_3(\varepsilon) = \tfrac{\sqrt{3\varepsilon^2+6}}{6} - \tfrac{\varepsilon\sqrt{3}}{2}, \tag{76}$$

$$A(\varepsilon) = 2\pi f_1(\varepsilon) h(\varepsilon) = \tfrac{\pi(3\varepsilon^2+6) - 9\pi\varepsilon\sqrt{\varepsilon^2+2}}{18}. \tag{77}$$

The corresponding *area defect* is a normalized version of (24), namely the normalized area of the sphere minus twice the normalized area of the caps:

$$\Delta(\varepsilon) = \tfrac{4\pi f_1^2(\varepsilon) - 4A(\varepsilon)}{\varepsilon} = -\tfrac{\pi\varepsilon}{3} - \tfrac{2\pi}{3\varepsilon} + 2\pi\sqrt{\varepsilon^2+2}. \tag{78}$$

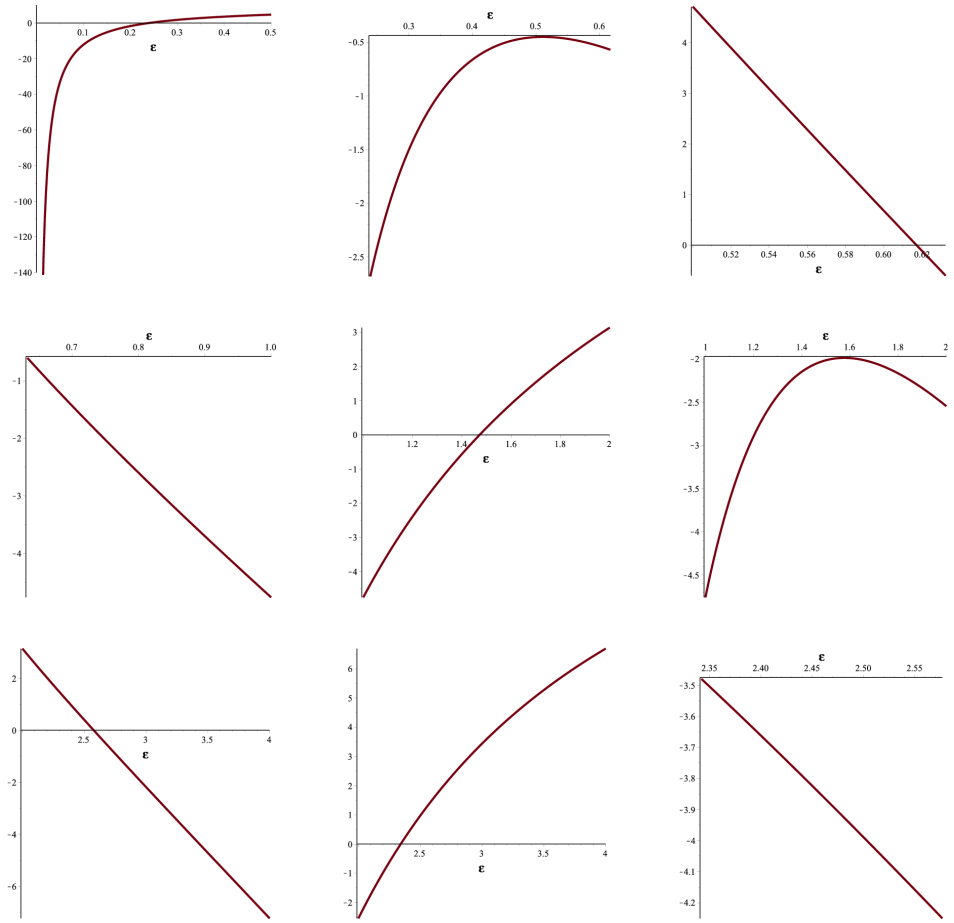

FIG. 9. *The graphs of the area defect taken at strategic critical radii.* Top row *from* left *to* right*: at the second critical radius in the interval* $(0.00, 0.50]$*, at the third critical radius in* $[0.239\ldots, 0.632\ldots]$*, at the second critical radius in* $[0.50, 0.632\ldots]$. Middle row *from* left *to* right*: at the second critical radius in* $[0.632\ldots, 1.00]$*, at the second and third critical radii in* $[1.00, 2.00]$. Bottom row *from* left *to* right*: at the second and third critical radii in* $[2.00, \infty)$*, at the fourth critical radius in* $[2.342\ldots, 2.576\ldots]$.

With the help of the Maple software [20], we find that the area defect is negative for $0 < \varepsilon < \sqrt{70}/35 = 0.239\ldots$ and positive in the complementary open interval; see Figure 9, left graph in top row. We therefore divide the considered interval into two, namely into $(0, 0.239\ldots]$ corresponding to Case I and $[0.239\ldots, 0.5]$ corresponding to Case II; see Table 1. In Case I, the equilibrium radius lies between the first two critical radii, and the search is complete. In Case II, the equilibrium radius lies to the right of the second critical radius, and we continue the search by evaluating the area defect at the third critical radius, $f_2(\varepsilon)$. At this size, the ball intersects six additional facets of the Voronoi domain, all at distance $f_1(\varepsilon)$ from the origin. We thus deal with two types of caps and index their heights and areas by the subscript of the corresponding critical radius:

$$h_3(\varepsilon) = f_2(\varepsilon) - f_3(\varepsilon) = \frac{\sqrt{12\varepsilon^2+6}}{6} - \frac{\varepsilon\sqrt{3}}{2}, \tag{79}$$

$$h_1(\varepsilon) = f_2(\varepsilon) - f_1(\varepsilon) = \frac{\sqrt{12\varepsilon^2+6}}{6} - \frac{\sqrt{3\varepsilon^2+6}}{6}, \tag{80}$$

$$A_3(\varepsilon) = 2\pi f_2(\varepsilon) h_3(\varepsilon) = \tfrac{\pi\sqrt{12\varepsilon^2+6}}{3}\,\tfrac{\sqrt{12\varepsilon^2+6}-3\sqrt{3}\varepsilon}{6}, \tag{81}$$

$$A_1(\varepsilon) = 2\pi f_2(\varepsilon) h_1(\varepsilon) = \tfrac{\pi\sqrt{12\varepsilon^2+6}}{3}\,\tfrac{\sqrt{12\varepsilon^2+6}-\sqrt{3\varepsilon^2+6}}{6}. \tag{82}$$

The corresponding area defect is

$$\begin{aligned}\Delta(\varepsilon) &= \tfrac{4\pi f_2^2(\varepsilon) - 4A_3(\varepsilon) - 12A_1(\varepsilon)}{\varepsilon} \\ &= -\tfrac{14\pi(2\varepsilon^2+1)}{3\varepsilon} + \tfrac{2\pi\sqrt{4\varepsilon^2+2}(\varepsilon+\sqrt{\varepsilon^2+2})}{\varepsilon},\end{aligned} \tag{83}$$

which is negative for every ε in the considered interval; see Figure 9, middle graph in top row. It follows that in Case II, the equilibrium radius lies between the second and third critical radii.

Second sequence. For $0.5 \le \varepsilon \le \sqrt{2/5} = 0.632\ldots$, the sorted sequence of critical radii is $f_1(\varepsilon) \le f_3(\varepsilon) \le f_2(\varepsilon) \le e_1(\varepsilon) \le e_2(\varepsilon) \le v_1(\varepsilon)$. As before, we begin the search at the second critical radius. The corresponding ball intersects six Voronoi facets, all at distance $f_1(\varepsilon)$ from the origin. Using (44) and (46), we get the height, cap area, and area defect as

$$h(\varepsilon) = f_3(\varepsilon) - f_1(\varepsilon) = \tfrac{\varepsilon\sqrt{3}}{2} - \tfrac{\sqrt{3\varepsilon^2+6}}{6}, \tag{84}$$

$$A(\varepsilon) = 2\pi f_3(\varepsilon) h(\varepsilon) = \tfrac{\pi\varepsilon(3\varepsilon-\sqrt{\varepsilon^2+2})}{2}, \tag{85}$$

$$\Delta(\varepsilon) = \tfrac{4\pi f_3^2(\varepsilon) - 12A(\varepsilon)}{\varepsilon} = -15\pi\varepsilon + 2\pi\sqrt{9\varepsilon^2+18}. \tag{86}$$

The last is positive for $\varepsilon < 2\sqrt{42}/21 = 0.617\ldots$ and negative for values of ε larger than this bound; see Figure 9, right graph in top row. We thus divide the considered interval into $[0.5, 0.617\ldots]$ corresponding to Case III and $[0.617\ldots, 0.632\ldots]$ corresponding to Case IV. In Case IV, the equilibrium radius lies between the first two critical radii, and the search is complete. In Case III, we continue by evaluating the area defect at $f_2(\varepsilon)$, at which size the ball intersects two additional Voronoi facets at distance $f_3(\varepsilon)$ from the origin. The corresponding formulas for the height, cap area, and area defect are the same as (79)–(83). Again, the area defect is negative, which implies that the equilibrium radius is between $f_3(\varepsilon)$ and $f_2(\varepsilon)$; compare with Table 1.

Third sequence. For $0.632\ldots \le \varepsilon \le \sqrt{19-3\sqrt{33}}/2 = 0.664\ldots$, the sorted sequence of critical radii is $f_1(\varepsilon) \le f_2(\varepsilon) \le f_3(\varepsilon) \le e_1(\varepsilon) \le e_2(\varepsilon) \le v_1(\varepsilon)$. Beginning the search at $f_2(\varepsilon)$, the ball intersects six Voronoi facets, all at distance $f_1(\varepsilon)$ from the origin. Using (44) and (45), we get

$$h(\varepsilon) = f_2(\varepsilon) - f_1(\varepsilon) = \tfrac{\sqrt{12\varepsilon^2+6}-\sqrt{3\varepsilon^2+6}}{6}, \tag{87}$$

$$A(\varepsilon) = 2\pi f_2(\varepsilon) h(\varepsilon) = \tfrac{\pi(4\varepsilon^2+2-\sqrt{2(2\varepsilon^2+1)(\varepsilon^2+2)})}{6}, \tag{88}$$

$$\Delta(\varepsilon) = \tfrac{4\pi f_2^2(\varepsilon) - 12A(\varepsilon)}{\varepsilon} = \tfrac{2\pi(-10\varepsilon^2-5+\sqrt{12\varepsilon^2+6}\sqrt{3\varepsilon^2+6})}{3\varepsilon} \tag{89}$$

for the height, cap area, and area defect. The last is negative for $\varepsilon > \sqrt{22}/8 \approx 0.59$ and therefore within the entire considered interval. In other words, in Case V the equilibrium radius lies between the first and the second critical radii; compare with Table 1.

Fourth sequence. For $0.664\ldots \le \varepsilon \le 1$, the sorted sequence of critical radii is $f_1(\varepsilon) \le f_2(\varepsilon) \le e_1(\varepsilon) \le f_3(\varepsilon) \le e_2(\varepsilon) \le v_1(\varepsilon)$. Beginning the search at $f_2(\varepsilon)$, we get the same formulas for the height, cap area, and area defect as in (87)–(89). The area defect is negative in the entire interval; see Figure 9, left graph in middle row. If follows that in Case VI the equilibrium radius lies between the first two critical radii; compare with Table 1.

Fifth sequence. For $1 \le \varepsilon \le 2$, the sorted sequence of critical radii is $f_1(\varepsilon) \le f_4(\varepsilon) \le e_4(\varepsilon) \le e_3(\varepsilon) \le v_2(\varepsilon) \le v_3(\varepsilon)$. Beginning the search at $f_4(\varepsilon)$, the ball intersects six Voronoi facets, all at distance $f_1(\varepsilon)$ from the origin. Using (50) and (51), we get

$$h(\varepsilon) = f_4(\varepsilon) - f_1(\varepsilon) = \tfrac{\sqrt{2}}{2} - \tfrac{\sqrt{3\varepsilon^2+6}}{6}, \tag{90}$$

$$A(\varepsilon) = 2\pi f_4(\varepsilon) h(\varepsilon) = \tfrac{\sqrt{2}\pi}{6}\left(3\sqrt{2} - \sqrt{3\varepsilon^2+6}\right), \tag{91}$$

$$\Delta(\varepsilon) = \tfrac{4\pi f_4^2(\varepsilon) - 12A(\varepsilon)}{\varepsilon} = \tfrac{2\pi\left(\sqrt{6\varepsilon^2+12}-5\right)}{\varepsilon} \tag{92}$$

for the height, cap area, and area defect. The last is negative for $\varepsilon < \sqrt{13/6} = 1.471\ldots$ and positive for values of ε larger than this bound; see Figure 9, middle graph in middle row. We thus divide the considered interval into $[1, 1.471\ldots]$ corresponding to Case VII and $[1.471\ldots, 2]$ corresponding to Case VIII. In Case VII, the equilibrium radius lies between the first two critical radii, and the search is complete; compare with Table 1. In Case VIII, we continue the search with $e_4(\varepsilon)$, at which size the ball intersects all 12 Voronoi facets, six each at distances $f_1(\varepsilon)$ and $f_4(\varepsilon)$ from the origin. The heights and areas of the two types of caps and the area defect are

$$h_1(\varepsilon) = e_4(\varepsilon) - f_1(\varepsilon) = \tfrac{\varepsilon^2+2}{\sqrt{6(2\varepsilon^2+1)}} - \tfrac{\sqrt{3\varepsilon^2+6}}{6}, \tag{93}$$

$$h_4(\varepsilon) = e_4(\varepsilon) - f_4(\varepsilon) = \tfrac{\varepsilon^2+2}{\sqrt{6(2\varepsilon^2+1)}} - \tfrac{\sqrt{2}}{2}, \tag{94}$$

$$A_1(\varepsilon) = 2\pi e_4(\varepsilon) h_1(\varepsilon) = \tfrac{\pi(\varepsilon^2+2)^2}{3(2\varepsilon^2+1)} - \tfrac{\pi(\varepsilon^2+2)\sqrt{\varepsilon^2+2}}{\sqrt{18(2\varepsilon^2+1)}}, \tag{95}$$

$$A_4(\varepsilon) = 2\pi e_4(\varepsilon) h_4(\varepsilon) = \tfrac{\pi(\varepsilon^2+2)^2}{3(2\varepsilon^2+1)} - \tfrac{\pi(\varepsilon^2+2)}{\sqrt{3(2\varepsilon^2+1)}}, \tag{96}$$

$$\begin{aligned}\Delta(\varepsilon) &= \tfrac{4\pi e_4^2(\varepsilon) - 12A_1(\varepsilon) - 12A_4(\varepsilon)}{\varepsilon} \\ &= \tfrac{2\sqrt{2}\pi(\varepsilon^2+2)(\sqrt{\varepsilon^2+2}+\sqrt{6})}{\varepsilon\sqrt{2\varepsilon^2+1}} - \tfrac{22\pi(\varepsilon^2+2)^2}{3\varepsilon(2\varepsilon^2+1)}.\end{aligned} \tag{97}$$

It is negative over the entire interval; see Figure 9, right graph in middle row. It follows that in Case VIII, the equilibrium radius lies between the second and the third critical radii; compare with Table 1.

Sixth sequence. For $2 \le \varepsilon \le \sqrt{6} = 2.449\ldots$, the sorted sequence of critical radii is $f_4(\varepsilon) \le f_1(\varepsilon) \le e_3(\varepsilon) \le e_4(\varepsilon) \le v_2(\varepsilon) \le v_3(\varepsilon)$. Beginning the search at $f_1(\varepsilon)$, the ball intersects six Voronoi facets, all at distance $f_4(\varepsilon)$ from the origin. Using (50) and (51), we get

$$h(\varepsilon) = f_1(\varepsilon) - f_4(\varepsilon) = \tfrac{\sqrt{3\varepsilon^2+6}-3\sqrt{2}}{6}, \tag{98}$$

$$A(\varepsilon) = 2\pi f_1(\varepsilon) h(\varepsilon) = \tfrac{\pi(\varepsilon^2+2-\sqrt{6(\varepsilon^2+2)})}{6}, \tag{99}$$

$$\begin{aligned}\Delta(\varepsilon) &= \tfrac{4\pi f_1^2(\varepsilon) - 12A(\varepsilon)}{\varepsilon} \\ &= \tfrac{6\pi\sqrt{6(\varepsilon^2+2)}-5\pi\varepsilon^2-10\pi}{3\varepsilon}\end{aligned} \tag{100}$$

for the height, cap area, and area defect. The last is positive for all values of ε in the considered interval; see Figure 9, left graph in bottom row. We thus continue the search with $e_3(\varepsilon)$, at which size the ball intersects 12 Voronoi facets, six each at distances $f_4(\varepsilon)$ and $f_1(\varepsilon)$ from the origin. The corresponding heights, cap areas, and

area defect are

$$h_1(\varepsilon) = e_3(\varepsilon) - f_1(\varepsilon) = \tfrac{2\sqrt{6}-\sqrt{3\varepsilon^2+6}}{6}, \tag{101}$$

$$h_4(\varepsilon) = e_3(\varepsilon) - f_4(\varepsilon) = \tfrac{2\sqrt{6}-3\sqrt{2}}{6}, \tag{102}$$

$$A_1(\varepsilon) = 2\pi e_3(\varepsilon) h_1(\varepsilon) = \tfrac{\pi(4-\sqrt{2\varepsilon^2+4})}{3}, \tag{103}$$

$$A_4(\varepsilon) = 2\pi e_3(\varepsilon) h_4(\varepsilon) = \tfrac{(4-2\sqrt{3})\pi}{3}, \tag{104}$$

$$\begin{aligned}\Delta(\varepsilon) &= \tfrac{4\pi e_3^2(\varepsilon) - 12A_1(\varepsilon) - 12A_4(\varepsilon)}{\varepsilon} \\ &= \tfrac{12\sqrt{2}\pi\sqrt{\varepsilon^2+2}+24\sqrt{3}\pi-88\pi}{3\varepsilon}.\end{aligned} \tag{105}$$

The last is negative for $\varepsilon < \sqrt{278 - 132\sqrt{3}}/3 = 2.342\ldots$ and positive for values of ε larger than this bound; see Figure 9, middle graph in bottom row. We thus divide the considered interval into $[2, 2.342\ldots]$ corresponding to Case IX and $[2.342\ldots, 2.449\ldots]$ corresponding to Case X. In Case IX, the equilibrium radius lies between the second and third critical radii, and the search is complete; see Table 1. In Case X, we continue the search with $e_4(\varepsilon)$, at which size the ball still intersects the same 12 Voronoi facets, but some of the corresponding caps overlap. As mentioned earlier, we ignore these overlaps by considering the simplified soft density. We get the same equations for the heights, cap areas, and area defect as above, (101)–(105), except that we substitute $e_4(\varepsilon)$ for $e_3(\varepsilon)$. We list the corresponding equations for completeness:

$$h_1(\varepsilon) = e_4(\varepsilon) - f_1(\varepsilon) = \tfrac{\varepsilon^2+2}{\sqrt{6(2\varepsilon^2+1)}} - \tfrac{\sqrt{3\varepsilon^2+6}}{6}, \tag{106}$$

$$h_4(\varepsilon) = e_4(\varepsilon) - f_4(\varepsilon) = \tfrac{\varepsilon^2+2}{\sqrt{6(2\varepsilon^2+1)}} - \tfrac{\sqrt{2}}{2}, \tag{107}$$

$$A_1(\varepsilon) = 2\pi e_4(\varepsilon) h_1(\varepsilon) = \tfrac{\pi(\varepsilon^2+2)^2}{3(2\varepsilon^2+1)} - \tfrac{\pi(\varepsilon^2+2)\sqrt{3\varepsilon^2+6}}{3\sqrt{6(2\varepsilon^2+1)}}, \tag{108}$$

$$A_4(\varepsilon) = 2\pi e_4(\varepsilon) h_4(\varepsilon) = \tfrac{\pi(\varepsilon^2+2)^2}{3(2\varepsilon^2+1)} - \tfrac{\pi(\varepsilon^2+2)}{\sqrt{3(2\varepsilon^2+1)}}, \tag{109}$$

$$\begin{aligned}\Delta(\varepsilon) &= \tfrac{4\pi e_4^2(\varepsilon) - 12A_1(\varepsilon) - 12A_4(\varepsilon)}{\varepsilon} \\ &= \tfrac{\pi(6\sqrt{2(\varepsilon^2+2)(2\varepsilon^2+1)}+12\sqrt{6\varepsilon^2+3}-22\varepsilon^2-44)(\varepsilon^2+2)}{3\varepsilon(2\varepsilon^2+1)}.\end{aligned} \tag{110}$$

The area defect is negative for all $\varepsilon > 0$, which covers the interval of interest; see Figure 9, right graph in bottom row. It follows that in Case X, the equilibrium radius lies between $e_3(\varepsilon)$ and $e_4(\varepsilon)$; compare with Table 1.

Last sequence. For $2.449\ldots \le \varepsilon < \infty$, the sorted sequence of critical radii is $f_4(\varepsilon) \le e_3(\varepsilon) \le f_1(\varepsilon) \le e_4(\varepsilon) \le v_2(\varepsilon) \le v_3(\varepsilon)$. Beginning the search at $e_3(\varepsilon)$, the ball intersects six Voronoi facets, all at distance $f_4(\varepsilon)$ from the origin. Using (51) and (52), we get

$$h(\varepsilon) = e_3(\varepsilon) - f_4(\varepsilon) = \tfrac{2\sqrt{6}-3\sqrt{2}}{6}, \tag{111}$$

$$A(\varepsilon) = 2\pi e_3(\varepsilon) h(\varepsilon) = \tfrac{(4-2\sqrt{3})\pi}{3}, \tag{112}$$

$$\Delta(\varepsilon) = \tfrac{4\pi e_3^2(\varepsilon) - 12A(\varepsilon)}{\varepsilon} = \tfrac{8\pi(3\sqrt{3}-5)}{3\varepsilon} \tag{113}$$

for the height, cap area, and area defect. The last is positive over the entire interval. We thus continue the search at $f_1(\varepsilon)$. Ignoring overlaps by considering the simplified soft density, we get the same formulas as in (98)–(100). The area defect is positive

for $\varepsilon < \sqrt{166}/5 = 2.576\ldots$ and negative for ε exceeding this bound; see Figure 9, left graph in bottom row. We thus divide the interval into $[2.449\ldots, 2.576\ldots]$ corresponding to Case XI and $[2.576\ldots, \infty)$ corresponding to Case XII. In Case XII, the equilibrium radius lies between $e_3(\varepsilon)$ and $f_1(\varepsilon)$, and the search is complete; compare with Table 1. In Case XI, we continue the search at $e_4(\varepsilon)$. Ignoring overlaps among the caps, we get the same formulas as in (106)–(110). The area defect is negative for all values of ε in the interval of interest; see Figure 9, right graph in bottom row. It follows that the equilibrium radius in Case XI is between $f_1(\varepsilon)$ and $e_4(\varepsilon)$; compare with Table 1.

A.3. Maximum soft density. After identifying the position of the equilibrium radius among the critical radii in Appendix A.2, we now compute the equilibrium radius as well as the corresponding soft density. By construction, this is the maximum soft density for any given parameter ε and thus gives the graph displayed in Figure 7. We consider Cases I–XII in turn but consolidate the 12 cases to five.

Case I. Referring to Table 1, we recall that for all $\varepsilon \in (0, 0.239\ldots]$, the equilibrium radius lies between the first two critical radii: $f_3(\varepsilon) \le \varrho(\varepsilon) \le f_1(\varepsilon)$. We get an equation for the equilibrium radius by setting the area defect to zero. Note that the height, cap area, and area defect are

$$h_3(\varepsilon) = \varrho(\varepsilon) - f_3(\varepsilon) = \varrho(\varepsilon) - \tfrac{\sqrt{3}\varepsilon}{2}, \tag{114}$$

$$A_3(\varepsilon) = 2\pi\varrho(\varepsilon)h_3(\varepsilon) = 2\pi\varrho(\varepsilon)\left(\varrho(\varepsilon) - \tfrac{\sqrt{3}\varepsilon}{2}\right), \tag{115}$$

$$\Delta(\varepsilon) = \tfrac{4\pi\varrho^2(\varepsilon) - 4A_4(\varepsilon)}{\varepsilon} = \tfrac{4\pi\varrho(\varepsilon)[\sqrt{3}\varepsilon - \varrho(\varepsilon)]}{\varepsilon}. \tag{116}$$

Setting $\Delta(\varepsilon) = 0$, we get $\varrho(\varepsilon) = \sqrt{3}\varepsilon$; compare with (56). To get the soft density, we still need the volume of the cap, by which we mean the volume of the convex hull of the cap. Equivalently, it is the volume of the cone over the cap minus the volume of the cone of the disk spanned by the circle bounding the cap. The area of the disk is $2\pi h_3(\varepsilon)\varrho(\varepsilon) - \pi h_3^2(\varepsilon)$. The volume of the cap and the soft density are therefore

$$V_3(\varepsilon) = \tfrac{\pi[3h_3^2(\varepsilon)\varrho(\varepsilon) - h_3^3(\varepsilon)]}{3} \tag{117}$$

$$= \tfrac{\pi[\varepsilon\sqrt{3} - 2\varrho(\varepsilon)]^2[\varepsilon\sqrt{3} + 4\varrho(\varepsilon)]}{24}, \tag{118}$$

$$\delta_1(\varepsilon) = \tfrac{4\pi\varrho^3(\varepsilon) - 12V_3(\varepsilon)}{3\varepsilon} = \tfrac{3\sqrt{3}\pi\varepsilon^2}{2}; \tag{119}$$

compare with (57).

Cases II–III. Referring to Table 1, we note that for every $\varepsilon \in [0.239\ldots, 0.617\ldots]$ the ball with the equilibrium radius intersects the same eight Voronoi facets. Indeed, we have $f_3(\varepsilon), f_1(\varepsilon) \le \varrho(\varepsilon) \le f_2(\varepsilon)$ throughout the interval. To get an equation for the equilibrium radius, we reuse the equation for A_3 and compute the height and area of the other type of cap and the area defect:

$$h_1(\varepsilon) = \varrho(\varepsilon) - f_1(\varepsilon) = \varrho(\varepsilon) - \tfrac{\sqrt{\varepsilon^2+2}}{2\sqrt{3}}, \tag{120}$$

$$A_1(\varepsilon) = 2\pi\varrho(\varepsilon)h_1(\varepsilon) = 2\pi\varrho(\varepsilon)\left(\varrho(\varepsilon) - \tfrac{\sqrt{\varepsilon^2+2}}{2\sqrt{3}}\right), \tag{121}$$

$$\Delta(\varepsilon) = \tfrac{4\pi\varrho^2(\varepsilon) - 4A_3(\varepsilon) - 12A_1(\varepsilon)}{\varepsilon} \tag{122}$$

$$= \tfrac{4\pi\varrho(\varepsilon)[\sqrt{3}\varepsilon - \sqrt{3\varepsilon^2+6} - 7\varrho(\varepsilon)]}{\varepsilon}. \tag{123}$$

Setting $\Delta(\varepsilon) = 0$, we get $\varrho(\varepsilon) = \left(\sqrt{3}\varepsilon + \sqrt{3\varepsilon^2 + 6}\right)/7$; compare with (58). As before, we continue by computing the volume of the cap and the soft density:

$$\begin{aligned} V_1(\varepsilon) &= \tfrac{\pi[3h_1^2(\varepsilon)\varrho(\varepsilon) - h_1^3(\varepsilon)]}{3} \\ &= \tfrac{\pi[-6\varrho(\varepsilon)+\sqrt{3\varepsilon^2+6}]^2[12\varrho(\varepsilon)+\sqrt{3\varepsilon^2+6}]}{648}, \end{aligned} \tag{124}$$

$$\begin{aligned} \delta_1(\varepsilon) &= \tfrac{4\pi\varrho^3(\varepsilon) - 12V_3(\varepsilon) - 36V_1(\varepsilon)}{3\varepsilon} \\ &= -\tfrac{\pi[27\sqrt{3}\varepsilon(11\varepsilon^2-8)+(26-95\varepsilon^2)\sqrt{3\varepsilon^2+6}]}{882\varepsilon}; \end{aligned} \tag{125}$$

compare with (59). The only root of the derivative is $\delta_1{}'(0.5) = 0$, with the second derivative $\delta_1{}''(0.5) < 0$. We see in Figure 10 that the second derivative is negative throughout the interval of interest, which implies that the maximum soft density is concave over $[0.239\ldots, 0.617\ldots]$; see Figure 7.

Cases IV–VII. Referring to Table 1, we note that for every $\varepsilon \in [0.617\ldots, 1.471\ldots]$ the ball with the equilibrium radius intersects the same six Voronoi facets: $f_1(\varepsilon) \leq \varrho(\varepsilon) \leq f_2(\varepsilon), f_3(\varepsilon), f_4(\varepsilon)$ throughout the interval. Reusing (121), the area defect is

$$\Delta(\varepsilon) = \tfrac{4\pi\varrho^2(\varepsilon) - 12A_1(\varepsilon)}{\varepsilon} = \tfrac{4\pi\varrho(\varepsilon)\sqrt{3\varepsilon^2+6} - 20\pi\varrho^2(\varepsilon)}{\varepsilon}. \tag{126}$$

Setting $\Delta(\varepsilon) = 0$, we get $\varrho(\varepsilon) = \sqrt{3\varepsilon^2 + 6}/5$; compare with (60). Reusing (124), the soft density is

$$\delta_1(\varepsilon) = \tfrac{4\pi\varrho^3(\varepsilon) - 36V_1(\varepsilon)}{3\varepsilon} = \tfrac{11\pi\sqrt{(3\varepsilon^2+6)^3}}{1350\varepsilon}; \tag{127}$$

compare with (61). The only root of the derivative is $\delta_1{}'(1) = 0$, with the second derivative $\delta_1{}''(1) > 0$. We see in Figure 11 that the second derivative is positive throughout the interval of interest, which implies that the maximum soft density is convex over $[0.617\ldots, 1.471\ldots]$; see Figure 7.

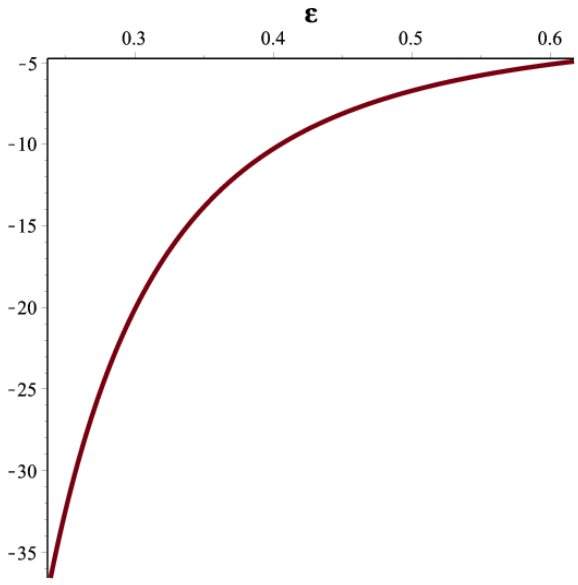

FIG. 10. *The second derivative of the maximum soft density function within the interval* $[0.239\ldots, 0.617\ldots]$.

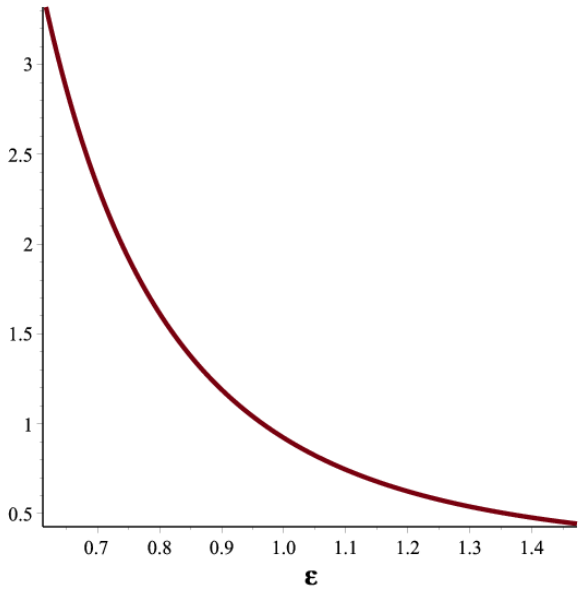

FIG. 11. *The second derivative of the maximum soft density function within the interval* $[0.617\ldots, 1.471\ldots]$.

Cases VIII–XI. Referring to Table 1, we note that for $\varepsilon \in [1.471\ldots, 2.576\ldots]$ the ball with the equilibrium radius intersects all 12 Voronoi facets: $f_1(\varepsilon), f_4(\varepsilon) \le \varrho(\varepsilon)$. In Cases X–XI, there are overlaps among the corresponding caps, but we ignore them for the time being by considering the simplified soft density. We reuse (121) and compute the height and area of the remaining cap type and the area defect:

$$h_4(\varepsilon) = \varrho(\varepsilon) - f_4(\varepsilon) = \varrho(\varepsilon) - \tfrac{\sqrt{2}}{2}, \tag{128}$$

$$A_4(\varepsilon) = 2\pi\varrho(\varepsilon)h_4(\varepsilon) = 2\pi\varrho(\varepsilon)\left(\varrho(\varepsilon) - \tfrac{\sqrt{2}}{2}\right), \tag{129}$$

$$\begin{aligned}\Delta(\varepsilon) &= \tfrac{4\pi\varrho^2(\varepsilon) - 12A_1(\varepsilon) - 12A_4(\varepsilon)}{\varepsilon} \\ &= \tfrac{12\sqrt{2}\pi\varrho(\varepsilon) + 4\pi\varrho(\varepsilon)\sqrt{3\varepsilon^2+6} - 44\pi\varrho^2(\varepsilon)}{\varepsilon}.\end{aligned} \tag{130}$$

Setting $\Delta(\varepsilon) = 0$, we get $\varrho(\varepsilon) = \left(\sqrt{3\varepsilon^2+6} + 3\sqrt{2}\right)/11$; compare with (62). We continue by computing the cap volume and the simplified soft density:

$$\begin{aligned}V_4(\varepsilon) &= \tfrac{\pi(3\varrho(\varepsilon)h_4^2(\varepsilon) - h_4^3(\varepsilon))}{3} \\ &= \tfrac{\pi(\sqrt{2} - 2\varrho(\varepsilon))^2(4\varrho(\varepsilon) + \sqrt{2})}{24},\end{aligned} \tag{131}$$

$$\begin{aligned}\delta_{1\mathrm{s}}(\varepsilon) &= \tfrac{4\pi\varrho^3(\varepsilon) - 36V_1(\varepsilon) - 36V_4(\varepsilon)}{3\varepsilon} \\ &= \tfrac{\pi[324\sqrt{2}\varepsilon^2 - 882\sqrt{2} + (478 - 85\varepsilon^2)\sqrt{3\varepsilon^2+6}]}{2178\varepsilon};\end{aligned} \tag{132}$$

compare with (63). The only root of the derivative is $\delta_{1\mathrm{s}}{}'(2) = 0$, with the second derivative $\delta_{1\mathrm{s}}{}''(2) < 0$. We see in Figure 12 that the second derivative is negative throughout the interval of interest, which implies that the maximum simplified soft density is concave over $[1.471\ldots, 2.576\ldots]$; see Figure 7. Interestingly, the second derivative does not go to 0 when ε approaches the endpoints, and we

observe the same phenomenon in Figures 10 and 11. It follows that the second derivative of the maximum simplified soft density has discontinuities, namely at $\varepsilon = 0.239\ldots, 0.617\ldots, 1.471\ldots, 2.576\ldots$.

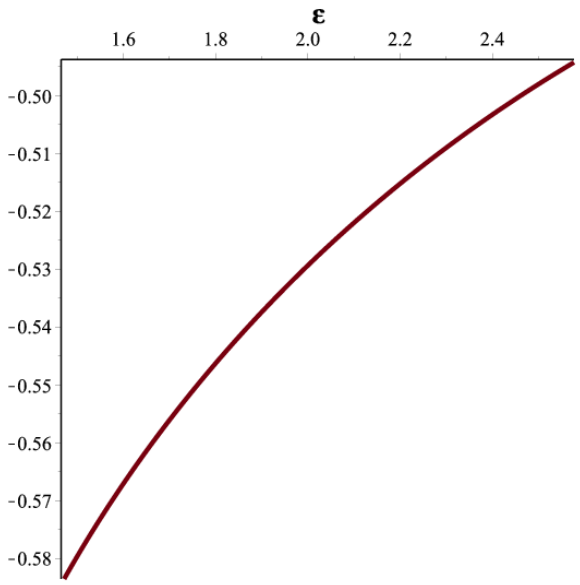

FIG. 12. *The second derivative of the maximum soft density function within the interval* $[1.471\ldots, 2.576\ldots]$.

Case XII. Referring to Table 1, we note that for $\varepsilon \in [2.576\ldots, \infty)$ the ball with the equilibrium radius intersects only six Voronoi facets: $f_4(\varepsilon) \leq \varrho(\varepsilon) \leq f_1(\varepsilon)$. Ignoring the overlaps among the corresponding caps, we consider the simplified soft density. Reusing (129), we get the area defect:

$$\Delta(\varepsilon) = \tfrac{4\pi\varrho^2(\varepsilon) - 12A_4(\varepsilon)}{\varepsilon} = \tfrac{12\sqrt{2}\pi\varrho(\varepsilon) - 20\pi\varrho^2(\varepsilon)}{\varepsilon}. \tag{133}$$

Setting $\Delta(\varepsilon) = 0$, we get $\varrho(\varepsilon) = 3\sqrt{2}/5$; compare with (64). Reusing (131), we get the simplified soft density:

$$\delta_{1s}(\varepsilon) = \tfrac{4\pi\varrho^3(\varepsilon) - 36V_4(\varepsilon)}{3\varepsilon} = \tfrac{11\sqrt{2}\pi}{25\varepsilon}; \tag{134}$$

compare with (65).

A.4. Unsimplified soft density. Here we consider equilibrium configurations with triple intersections. In particular, we recompute the position of the equilibrium radius among the critical radii for the unsimplified soft density, the threshold for ε beyond which the equilibrium radius remains constant, and the constant C such that the unsimplified soft density has the form (69).

Position of the equilibrium radius. For $\varepsilon > 2.342\ldots$, the position of the equilibrium radius for the soft density may be different from that for the simplified soft density. The reason is that the formula for the area defect now includes a term involving triple intersections. Considering Case X, we begin the search at $e_4(\varepsilon)$, at which size the ball at the origin intersects six Voronoi facets at distance $f_4(\varepsilon)$, six Voronoi

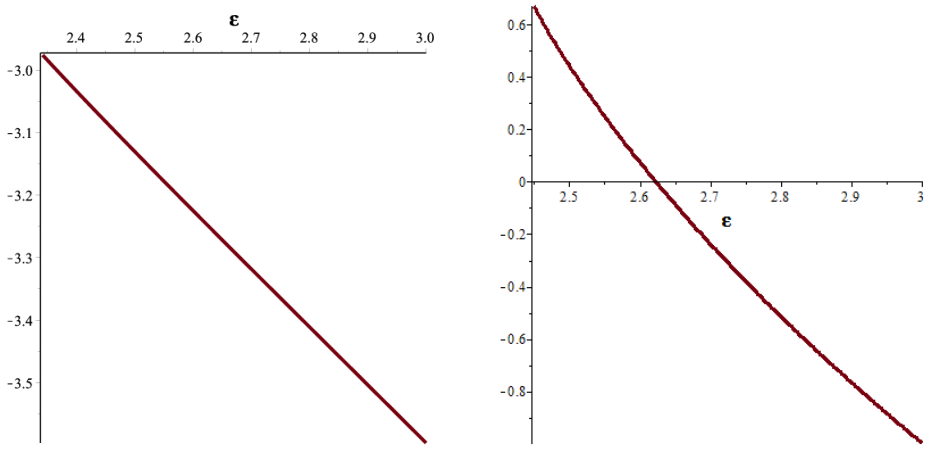

FIG. 13. *Two graphs of the area defect for the soft density measure, at* $e_4(\varepsilon)$ *for* $\varepsilon \in [2.342\ldots, 3]$ *on the* left *and at* $f_1(\varepsilon)$ *for* $\varepsilon \in [2.449\ldots, 3]$ *on the* right.

facets at distance $f_1(\varepsilon)$, and six Voronoi edges at distance $e_3(\varepsilon)$. Using the spherical area formula in [10] as well as (108) and (109), we get

$$A_e(\varepsilon) = \tfrac{b_1(\varepsilon)+b_2(\varepsilon)}{6\varepsilon^2+3}, \tag{135}$$

$$\begin{aligned}\Delta(\varepsilon) &= \tfrac{4\pi e_4^2(\varepsilon)-12A_1(\varepsilon)-12A_4(\varepsilon)+12A_e(\varepsilon)}{\varepsilon}\\ &= \tfrac{2[6b_1(\varepsilon)+6b_2(\varepsilon)+\pi(\varepsilon^2+2)b_3(\varepsilon)]}{\varepsilon(6\varepsilon^2+3)}\end{aligned} \tag{136}$$

for the surface area of a single triple intersection and the area defect, in which

$$\begin{aligned}b_1(\varepsilon) &= (\varepsilon^2+2)^2\left(\pi - \arccos\tfrac{\varepsilon^4-8\varepsilon^2-2}{2(\varepsilon^2-1)^2}\right),\\ b_2(\varepsilon) &= -2(\varepsilon^2+2)\sqrt{6\varepsilon^2+3}\arccos\tfrac{\sqrt{2\varepsilon^2+1}}{\varepsilon^2-1},\\ b_3(\varepsilon) &= 6\sqrt{6\varepsilon^2+3}+\sqrt{(12\varepsilon^2+6)(3\varepsilon^2+6)}-11(\varepsilon^2+2).\end{aligned} \tag{137}$$

The area defect is negative for all $\varepsilon > 2.342\ldots$; see the left graph in Figure 13. It follows that the equilibrium radius remains at the same position among the critical radii as for the simplified soft density. In Cases XI–XII, the expression for the area defect at $e_4(\varepsilon)$ is the same as above, which implies that the equilibrium radius is smaller than $e_4(\varepsilon)$. It remains to evaluate the area defect at $f_1(\varepsilon)$. Using (99), we get

$$A_f(\varepsilon) = c_1(\varepsilon) + c_2(\varepsilon), \tag{138}$$

$$\begin{aligned}\Delta(\varepsilon) &= \tfrac{4\pi f_1^2(\varepsilon)-12A_4(\varepsilon)+12A_f(\varepsilon)}{\varepsilon}\\ &= c_3(\varepsilon)+c_4(\varepsilon)\end{aligned} \tag{139}$$

for the surface area of the triple intersection and the area defect at radius $f_1(\varepsilon)$, in which

$$\begin{aligned}c_1(\varepsilon) &= -\tfrac{\varepsilon^2+2}{6}\arccos\tfrac{\varepsilon^2-10}{2\varepsilon^2-8},\\ c_2(\varepsilon) &= \tfrac{2\pi+\pi\varepsilon^2}{6} - \tfrac{\sqrt{6\varepsilon^2+12}}{3}\arccos\tfrac{2}{\sqrt{2\varepsilon^2-8}},\end{aligned}$$

$$c_3(\varepsilon) = \tfrac{2\pi+\pi\varepsilon^2}{3\varepsilon} - \tfrac{(2\varepsilon^2+4)}{\varepsilon} \arccos \tfrac{\varepsilon^2-10}{2\varepsilon^2-8},$$
$$c_4(\varepsilon) = \tfrac{2\sqrt{6\varepsilon^2+12}}{\varepsilon} \left[\pi - 2 \arccos \tfrac{2}{\sqrt{2\varepsilon^2-8}}\right].$$

As shown in Figure 13 on the right, $\varepsilon = 2.622758110\ldots \approx 2.62$ separates positive from negative area defect. In other words, Cases XI–XII remain the same, except that the transition shifts from $2.576\ldots$ to $2.622\ldots$.

Maximum soft density. Cases X–XI corresponding to $\varepsilon \in [2.342\ldots, 2.62\ldots]$ have the same expression for the area defect. Reusing (121) and (129), we get

$$A_e(\varepsilon) = -2\varrho(\varepsilon)[d_1(\varepsilon) + d_2(\varepsilon) - \pi\varrho(\varepsilon)], \tag{140}$$
$$\Delta(\varepsilon) = \tfrac{4\pi\varrho^2(\varepsilon)-12A_1(\varepsilon)-12A_4(\varepsilon)+12A_e(\varepsilon)}{\varepsilon}$$
$$= \tfrac{4\varrho(\varepsilon)[-6d_1(\varepsilon)+d_3(\varepsilon)+d_4(\varepsilon)-6d_2(\varepsilon)]}{\varepsilon} \tag{141}$$

for the area of the triple intersection and the area defect, in which

$$d_1(\varepsilon) = \sqrt{2} \arccos \tfrac{1}{\sqrt{6\varrho^2(\varepsilon)-3}},$$
$$d_2(\varepsilon) = \varrho(\varepsilon) \arccos \tfrac{\varrho^2(\varepsilon)-1}{2\varrho^2(\varepsilon)-1},$$
$$d_3(\varepsilon) = \pi\sqrt{3\varepsilon^2+6},$$
$$d_4(\varepsilon) = 3\sqrt{2}\pi - 5\pi\varrho(\varepsilon).$$

Setting $\Delta(\varepsilon) = 0$, we do not succeed in finding a closed-form expression for $\varrho(\varepsilon)$, but we are able to sample its value at discrete parameters ε. Reusing (124) and (131), we get

$$V_e(\varepsilon) = \tfrac{[1-6\varrho^2(\varepsilon)]d_1(\varepsilon)+2d_5(\varepsilon)-4\varrho^2(\varepsilon)d_2(\varepsilon)}{6}, \tag{142}$$
$$\delta_1(\varepsilon) = \tfrac{4\pi\varrho^3(\varepsilon)-36V_1(\varepsilon)-36V_4(\varepsilon)+36V_e(\varepsilon)}{3\varepsilon}$$
$$= -\tfrac{d_3(\varepsilon)d_7(\varepsilon)+d_1(\varepsilon)d_8(\varepsilon)+144\varrho^2(\varepsilon)d_2(\varepsilon)+6d_6(\varepsilon)}{18\varepsilon} \tag{143}$$

for the volume of a single triple intersection and the soft density, in which

$$d_5(\varepsilon) = \tfrac{6\pi\varrho^3(\varepsilon)+\sqrt{3\varrho^2(\varepsilon)-2}}{3},$$
$$d_6(\varepsilon) = 20\pi\varrho^3(\varepsilon) + 3\sqrt{2}\pi[1-6\varrho^2(\varepsilon)] - 4\sqrt{3\varrho^2(\varepsilon)-2},$$
$$d_7(\varepsilon) = \varepsilon^2 - 36\varrho^2(\varepsilon) + 2,$$
$$d_8(\varepsilon) = 216\varrho^2(\varepsilon) - 36.$$

We use the ability to sample the equilibrium radius from (141) and plug these values into (143) to sketch the graph of $\delta_1(\varepsilon)$ in the interval $[2.342\ldots, 2.62\ldots]$, which falls, of course, between the graphs of the simplified and the extrapolated soft densities; see Figure 8.

Extrapolated soft density. In Case XII, the equilibrium radius is constant over the entire interval from $2.62\ldots$ to infinity. Reusing (129) and (140), we get

$$\Delta(\varepsilon) = \tfrac{4\pi\varrho^2(\varepsilon)-12A_4(\varepsilon)+12A_e(\varepsilon)}{\varepsilon}$$
$$= \tfrac{4\varrho(\varepsilon)[\pi\varrho(\varepsilon)+3\sqrt{2}\pi-6d_1(\varepsilon)-6d_2(\varepsilon)]}{\varepsilon} \tag{144}$$

for the area defect. Setting $\Delta(\varepsilon) = 0$ and reusing (131) and (142), we get

$$\varrho(\varepsilon) = 0.8601773122\ldots, \tag{145}$$

$$\delta_1(\varepsilon) = \frac{4\pi\varrho^3(\varepsilon) - 36V_4(\varepsilon) + 36V_e(\varepsilon)}{3\varepsilon}$$

$$= \frac{[6 - 36\varrho^2(\varepsilon)]d_1(\varepsilon) - 24\varrho^2(\varepsilon)d_2(\varepsilon) + d_9(\varepsilon)}{3\varepsilon}, \tag{146}$$

in which

$$d_9(\varepsilon) = 4\sqrt{3\varrho^2(\varepsilon) - 2} + 4\pi\varrho^3(\varepsilon) + 3\sqrt{2}\pi[6\varrho^2(\varepsilon) - 1].$$

Plugging the constant equilibrium radius (145) into (146), we get $\delta_1(\varepsilon) = C/\varepsilon$, with $C = 1.962290082\ldots \approx 1.96$; see Figure 8. This gives $\delta_{1\mathrm{x}}(2.342\ldots) = 0.8378301951\ldots$, which is less than the soft density of the FCC lattice at equilibrium, as desired.

Acknowledgments. We thank Robert Connelly and Vitaliy Kurlin for discussions on the topic of this paper, Georg Osang for telling us that the Brillouin zones were discovered long ago, and Hubert Wagner for creating for us the 3-dimensional plot in Figure 6. Furthermore, we thank Michael Kerber for proofreading the Maple file containing our computations and for help in using the CGAL library for generating the generalized Voronoi domains. Last, but not least, we thank the reviewers of this paper for their comments and for suggesting relevant additional references.

REFERENCES

[1] J. Balázs, *Über ein Kreisüberdeckungsproblem*, Acta Math. Acad. Sci. Hungar., 24 (1973), pp. 377–382.

[2] K. Bezdek and Z. Lángi, *Density bounds for outer parallel domains of unit ball packings*, Proc. Steklov Inst. Math., 288 (2015), pp. 209–225.

[3] L. Bieberbach, *Über die Inhaltsgleichheit der Brillouinschen Zonen*, Monatsh. Math. Phys., 48 (1939), pp. 509–515.

[4] G. Blind and R. Blind, *Ein Kreisüberdeckungsproblem*, Studia Sci. Math. Hungar., 21 (1986), pp. 35–57.

[5] L. Brillouin, *Les électrons dans les métaux et le classement des ondes de de Broglie correspondantes*, Comptes Rendus Hebdomadaires des Séances de l'Académie des Sciences, 191 (1930), pp. 292–294.

[6] J. H. Conway and N. J. A. Sloane, *Sphere Packings, Lattices and Groups*, 3rd ed., Springer-Verlag, New York, 1999.

[7] T. Cremer, G. Kreth, H. Koester, R. H. A. Fink, R. Heintzmann, M. Cremer, I. Solovei, D. Zink, and C. Cremer, *Chromosome territories, interchromatin domain compartment, and nuclear matrix: An integrated view of the functional nuclear architecture*, Crit. Rev. Eukaryot. Gene Expr., 10 (2000), pp. 179–212.

[8] B. Csikós, *On the volume of flowers in space forms*, Geom. Dedicata, 86 (2001), pp. 59–79.

[9] J. Dixon, S. Selvaraj, F. Yue, A. Kim, Y. Li, Y. Shen, M. Hu, J. Liu, and B. Ren, *Topological domains in mammalian genomes identified by analysis of chromatin interactions*, Nature, 485 (2012), pp. 376–380.

[10] H. Edelsbrunner and P. Fu, *Measuring Space Filling Diagrams and Voids*, Molecular Biophysics Report UIUC-BI-MB-94-01, Beckman Institute, University of Illinois at Urbana-Champaign, Champaign, IL, 1994.

[11] H. Edelsbrunner, M. Iglesias-Ham, and V. Kurlin, *Relaxed disk packing*, in Online Proceedings of the Canadian Conference on Computational Geometry, 2015.

[12] H. Edelsbrunner and M. Kerber, *Covering and packing with spheres by diagonal distortion in* $\mathbb{R}^n$, in Rainbow of Computer Science, Lecture Notes in Comput. Sci. 6570, C. Calude, G. Rozenberg, and A. Salomaa, eds., Springer, Heidelberg, 2011, pp. 20–35.

[13] H. Edelsbrunner and M. Kerber, *Dual complexes of cubical subdivisions of* $\mathbb{R}^n$, Discrete Comput. Geom., 47 (2012), pp. 393–414.

[14] H. Edelsbrunner and R. Seidel, *Voronoi diagrams and arrangements*, Discrete Comput. Geom., 1 (1986), pp. 25–44.

[15] G. Fejes Toth, *Multiple packing and covering of the plane with circles*, Acta Math. Acad. Sci. Hungar., 27 (1976), pp. 135–140.
[16] G. Fejes Toth, *Multiple packing and covering of spheres*, Acta Math. Acad. Sci. Hungar., 34 (1979), pp. 165–176.
[17] L. Fejes Tóth, *Lagerungen in der Ebene, auf der Kugel und im Raum*, Grundlehren Math. Wiss. 65, Springer, Berlin, 1953.
[18] M. Iglesias-Ham, M. Kerber, and C. Uhler, *Sphere packing with limited overlap*, in Online Proceedings of the Canadian Conferece on Computational Geometry, 2014.
[19] G. Kreth, P. Edelmann, and C. Cremer, *Towards a dynamical approach for the simulation of large scale, cancer correlated chromatin structures*, Ital. J. Anat. Embryol., 106 (2001), pp. 21–30.
[20] *MAPLE* 17, Maplesoft, a division of Waterloo Maple Inc., Waterloo, ON, Canada.
[21] C. Radin, *The ground state for soft disks*, J. Statist. Physics, 26 (1981), pp. 365–373.
[22] R. Sibson, *A vector identity for the Dirichlet tessellation*, Math. Proc. Cambridge Philos. Soc., 87 (1980), pp. 151–155.